



**HAL**  
open science

## Thermoelectric Borides: Review and Future Perspectives

Kivanc Saglik, Busra Mete, Ilayda Terzi, Christophe Candolfi, Umut Aydemir

► **To cite this version:**

Kivanc Saglik, Busra Mete, Ilayda Terzi, Christophe Candolfi, Umut Aydemir. Thermoelectric Borides: Review and Future Perspectives. *Advanced Physics Research*, 2023, 2 (8), pp.2300010. 10.1002/apxr.202300010 . hal-04130631

**HAL Id: hal-04130631**

**<https://hal.science/hal-04130631>**

Submitted on 16 Jun 2023

**HAL** is a multi-disciplinary open access archive for the deposit and dissemination of scientific research documents, whether they are published or not. The documents may come from teaching and research institutions in France or abroad, or from public or private research centers.

L'archive ouverte pluridisciplinaire **HAL**, est destinée au dépôt et à la diffusion de documents scientifiques de niveau recherche, publiés ou non, émanant des établissements d'enseignement et de recherche français ou étrangers, des laboratoires publics ou privés.

# Thermoelectric Borides: Review and Future Perspectives

Kivanc Saglik, Busra Mete, Ilayda Terzi, Christophe Candolfi, and Umut Aydemir\*

The conversion of waste heat into electricity plays a vital role in energy harvesting since conventional non-renewable energy sources have been rapidly approaching the limit of utilization. The thermoelectric (TE) technology relies on converting temperature difference (or waste heat) into electricity or vice versa. The performance of TE materials is gauged by  $zT = S^2T/\rho\kappa$ , where  $S$ ,  $\rho$ ,  $\kappa$ , and  $T$  represent the Seebeck coefficient, the electrical resistivity, the total thermal conductivity, and the absolute temperature, respectively. Boron-based compounds are considered refractory materials due to their high melting points and advanced chemical and mechanical stability. Besides high thermal stability, many borides exhibit intrinsically low thermal conductivity. The discovery of good TE efficiency in boron carbides, where unexpectedly high Seebeck coefficients ( $S(T) \approx 250 \mu\text{VK}^{-1}$ ) are observed at high charge carrier densities ( $\approx 10^{21} \text{ cm}^{-3}$ ), has induced an intense curiosity for the TE properties of other boron-based compounds. Intermetallic borides with high boron content (>65 at%) are of particular interest among all known TE materials due to their great potential in TE generators, which can operate under extreme environmental conditions ( $T > 1000 \text{ K}$ ). This article reviews the TE properties of borides and state-of-art TE materials upon boron/borides doping.

## 1. Introduction

Over the last decades, changes in living standards, technological progress, and economic growth have resulted in towering dependency on energy resources. Extensively used carbon-based fuels yield hazardous chemicals, and such sources rapidly approach the limit of utilization. In addition, around two-thirds of the global energy is wasted during industrial processes. Hence, the direct conversion of waste heat into electricity enabled by thermoelectric materials plays a vital role in energy harvesting. This technology involves the use of n- and p-type semiconductors connected electrically in series and thermally in parallel.<sup>[1]</sup> In such a device (Figure 1), the temperature gradient is converted into electricity by the migration of charge carriers.<sup>[2]</sup> The performance of thermoelectric materials is evaluated by “the dimensionless thermoelectric figure of merit,”  $zT = S^2T/\rho\kappa$ , where  $S$ ,  $\rho$ ,  $\kappa$ , and  $T$  are the Seebeck coefficient (or thermopower), the electrical resistivity, the total thermal conductivity, and the

absolute temperature, respectively.<sup>[2]</sup> A good thermoelectric material is a poor conductor of heat and a good conductor of electricity. Since electrons and holes are also heat carriers, decreasing the electrical resistivity elevates the electronic contribution to the thermal conductivity and decreases the  $zT$ .<sup>[2]</sup> This interdependency of the three transport coefficients on the charge carrier density challenges the discovery and optimization of materials with high  $zT$  values. Although state-of-the-art thermoelectric materials with enhanced  $zT$  are available, they may deteriorate at high temperatures and/or contain toxic elements.<sup>[3,4]</sup> Boride-based materials are abundant, non-toxic, refractory, and mechanically stable. Thus, they are utilized at very high temperatures (typically above 1200 K) where commercially existing materials cannot be used.<sup>[5]</sup> This target temperature range is shown in Figure 2. The combination of unique properties allows borides to be employed in different applications, for example, batteries, nuclear energy, wind turbines, armor production, solid fuels, superconductors, biomaterials, and propellants.<sup>[6,7]</sup> In this review, the properties of several families of boride-containing compounds are discussed as possible candidates for thermoelectric applications in power generation.

Research on thermoelectric borides focuses on three main groups: metal borides ( $\text{MB}_2$ ,  $\text{MB}_4$ , and  $\text{MB}_6$ ), alpha-borides ( $\text{B}_4\text{C}$ , and  $\text{B}_{12}$ ), and beta-borides ( $\text{B}_{105}$ ). Some higher borides, namely  $\text{REB}_{50}$  and  $\text{REB}_{66}$ , have also been studied extensively

K. Saglik, B. Mete, I. Terzi  
 Graduate School of Sciences and Engineering  
 Koç University  
 Istanbul 34450, Turkey

K. Saglik, B. Mete, I. Terzi  
 Koç University Boron and Advanced Materials Application and Research  
 Center (KUBAM)  
 Istanbul 34450, Turkey

C. Candolfi  
 Institut Jean Lamour  
 Université de Lorraine Nancy Cedex  
 Nancy 54011, France

U. Aydemir  
 Department of Chemistry  
 Koç University  
 Sariyer, Istanbul 34450, Turkey  
 E-mail: uaydemir@ku.edu.tr

 The ORCID identification number(s) for the author(s) of this article can be found under <https://doi.org/10.1002/apxr.202300010>

© 2023 The Authors. Advanced Physics Research published by Wiley-VCH GmbH. This is an open access article under the terms of the Creative Commons Attribution License, which permits use, distribution and reproduction in any medium, provided the original work is properly cited.

DOI: 10.1002/apxr.202300010

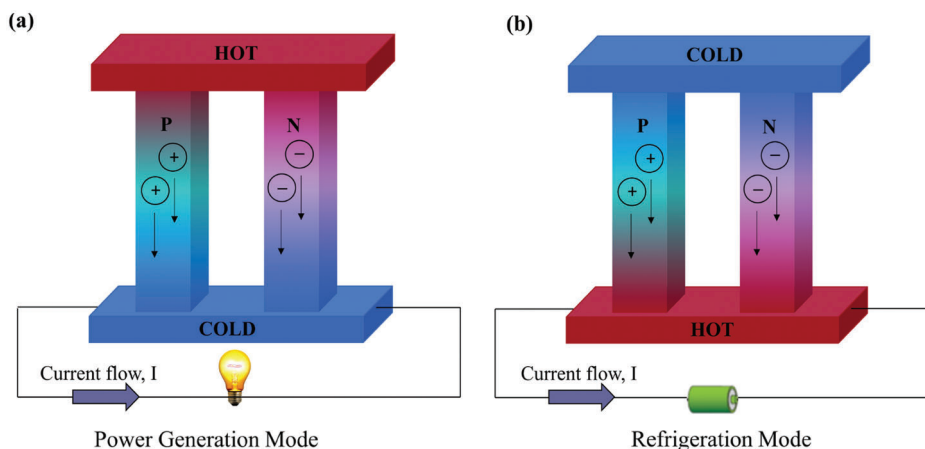


Figure 1. Operation principle of thermoelectric generators (TEGs).

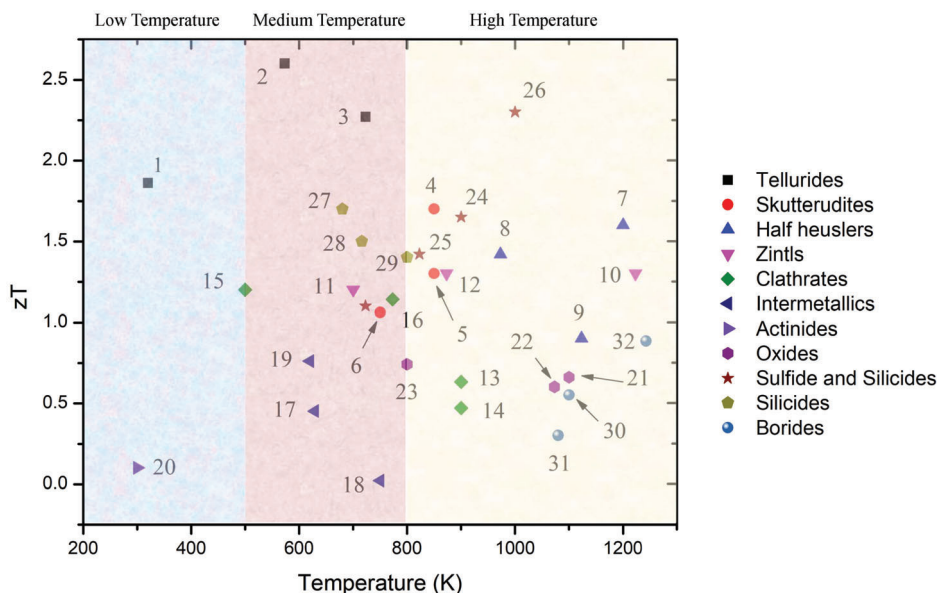


Figure 2. Commonly used families of thermoelectric materials with their peak  $zT$  values. [1]  $\text{Bi}_{0.5}\text{Sb}_{1.5}\text{Te}_3$ ,<sup>[3]</sup> 2)  $\text{Ge}_{0.87}\text{Pb}_{0.13}\text{Te}$ ,<sup>[4]</sup> 3)  $\text{Pb}_{0.953}\text{Na}_{0.04}\text{Ge}_{0.007}\text{Te}$ ,<sup>[8]</sup> 4)  $\text{Ba}_{0.08}\text{La}_{0.05}\text{Yb}_{0.08}\text{Co}_4\text{Sb}_{12}$ ,<sup>[9]</sup> 5)  $\text{Ce}_{0.14}\text{Co}_4\text{Sb}_{12}$ ,<sup>[10]</sup> 6)  $\text{Ce}_{0.45}\text{Nd}_{0.45}\text{Fe}_3\text{CoSb}_{12}$ ,<sup>[11]</sup> 7)  $(\text{Nb}_{0.6}\text{Ta}_{0.4})_{0.8}\text{Ti}_{0.2}\text{FeSb}$ ,<sup>[12]</sup> 8)  $\text{ZrCoBi}_{0.65}\text{Sb}_{0.15}\text{Sn}_{0.20}$ ,<sup>[13]</sup> 9)  $\text{Nb}_{0.83}\text{CoSb}$ ,<sup>[14]</sup> 10)  $\text{Yb}_{14}\text{MnSb}_{11}$ ,<sup>[15]</sup> 11)  $\text{YbCd}_2\text{Sb}_2$ ,<sup>[16]</sup> 12)  $\text{CaMg}_2\text{Bi}_2$ ,<sup>[16]</sup> 13)  $\text{Ba}_{6.4}\text{La}_{1.6}\text{Cu}_{16}\text{P}_{30}$ ,<sup>[17]</sup> 14)  $\text{Ba}_8\text{Al}_{16}\text{Ga}_2\text{Si}_{26}\text{P}_2$ ,<sup>[18]</sup> 15)  $\text{Ba}_8\text{Ga}_{10}\text{Al}_6\text{Sn}_{30}$ ,<sup>[19]</sup> 16)  $\text{Ba}_8\text{Ga}_{16}\text{Ge}_{30}$ ,<sup>[20]</sup> 17)  $\text{RuIn}_{2.950}\text{Zn}_{0.050}$ ,<sup>[21]</sup> 18)  $\text{FeGa}_{2.80}\text{Ge}_{0.20}$ ,<sup>[22]</sup> 19)  $\text{RuIn}_{2.975}\text{Zn}_{0.025}$ ,<sup>[23]</sup> 20)  $\text{Th}_3\text{P}_4$ ,<sup>[24]</sup> 21)  $\text{Sr}_{0.9}\text{La}_{0.1}\text{Ti}_{0.9}\text{Nb}_{0.1}\text{O}_3$ ,<sup>[25]</sup> 22)  $\text{Sr}_{0.95}(\text{Ti}_{0.8}\text{Nb}_{0.2})_{0.95}\text{Ni}_{0.05}\text{O}_3$ ,<sup>[26]</sup> 23)  $\text{Ca}_{2.5}\text{Tb}_{0.5}\text{Co}_4\text{O}_9$ ,<sup>[27]</sup> 24)  $\text{Pb}_{0.93}\text{Sb}_{0.05}\text{S}_{0.5}\text{Se}_{0.5}$ ,<sup>[28]</sup> 25)  $\text{Cu}_{1.85}\text{Ag}_{0.15}\text{Sn}_{0.9}\text{In}_{0.1}\text{Se}_3$ ,<sup>[29]</sup> 26)  $\text{Cu}_{1.94}\text{Se}_{0.5}\text{S}_{0.5}$ ,<sup>[30]</sup> 27)  $\text{Mg}_{1.98}\text{Cr}_{0.02}(\text{Si}_{0.3}\text{Sn}_{0.7})_{0.98}\text{Bi}_{0.02}$ ,<sup>[31]</sup> 28)  $\text{Mg}_{2.08}\text{Si}_{0.364}\text{Sn}_{0.6}\text{Sb}_{0.036}$ ,<sup>[32]</sup> 29)  $\text{Mg}_{2.16}(\text{Si}_{0.4}\text{Sn}_{0.6})_{0.97}\text{Bi}_{0.03}$ ,<sup>[33]</sup> 30)  $\text{B}_4\text{C} + 25 \text{ mol\% TiB}_2$ ,<sup>[34]</sup> 31)  $\text{SrB}_6$ ,<sup>[35]</sup> 32)  $\text{B}_{13}\text{C}_2$ .<sup>[36]</sup>

owing to their PGEC nature, making them good thermoelectric materials.<sup>[37]</sup> Metal borides mainly crystallize with a layered crystal structure and are mostly p-type semiconductors with high thermal conductivities, making them poor thermoelectrics.<sup>[38,39]</sup> Among these, only divalent hexaborides have shown promise owing to moderate  $S$  and  $\sigma$ .<sup>[6,38]</sup> On the other hand, diborides are very effective dopants, especially when added to boron carbides.<sup>[12]</sup> Due to the solubility of carbon in boron, boron carbides exhibit various appealing compositions because of superior mechanical properties, low thermal conductivities, and small electronic bandgap.<sup>[40,41]</sup> Additionally, their unexpectedly high Seebeck coefficient, along with ultra-high melting point

( $\approx 3036$  K), support the utilization of boron carbides under extreme conditions.<sup>[38]</sup> Having structural similarities, homologous series of rare-earth borocarbonitrides such as  $\text{REB}_{15.5}\text{CN}$ ,  $\text{REB}_{22}\text{C}_2\text{N}$ , and  $\text{REB}_{17}\text{CN}$  have drawn great attention as n-type counterparts of boron carbides which are p-type.<sup>[42]</sup> Alpha and beta polymorphs of boron constitute the skeleton of various compounds like  $\text{B}_{12}\text{As}_2$  or  $\text{B}_{105}$ .<sup>[43]</sup> Due to their excellent stability and the presence of vacancies in their crystal structure that enable tuning their physical properties,  $\beta$ -boron has been largely investigated.<sup>[44]</sup> In addition to high-temperature stability, they are mechanically robust thanks to the presence of directional B-B bonds.<sup>[45]</sup> The most striking discovery in this family is the

switching from p- to n-type conduction upon doping with V, Zr, or Cr.<sup>[46–48]</sup> In addition, elemental boron is a promising dopant for commercially available thermoelectric materials.<sup>[49–54]</sup> This review provides a detailed analysis of synthetic routes, thermoelectric properties of different families of borides as well as studies on state-of-the-art TE materials that have used elemental boron and boron compounds as dopants.

## 2. Synthesis Techniques of Borides

### 2.1. Polycrystalline Synthesis Methods

#### 2.1.1. Direct Reaction of the Elements

Under a protective atmosphere, for example, inert gas or vacuum, metal and boron powders are mixed in targeted stoichiometry and then reacted by heating at high temperatures.<sup>[55,56]</sup>



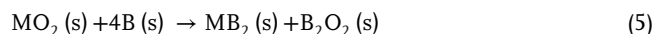
#### 2.1.2. Fast Heating and Sintering Methods

Since borides have high thermal stability, aside from commercial furnaces, other novel heating processes need to be employed to reach elevated temperatures such as arc-melting, inductively heating, hot press (HP), and spark plasma sintering (SPS). In the arc-melting process, metal and boron powders are melted in an argon atmosphere. Afterward, samples are annealed or ball-milled to obtain the target phase. Since boron is non-volatile and has high thermal resistance, arc melting is a prevalent method to obtain borides such as boron carbides,<sup>[36]</sup> tetraborides,<sup>[57]</sup> hexaborides,<sup>[58]</sup>  $\beta$ -boron,<sup>[45]</sup> and  $YB_{44}Si_2$ .<sup>[59]</sup> In induction heating, an electrically conductive material is heated by electromagnetic induction with a high-frequency alternating current, leading to heat generation by Eddy current. Stable boron nitride or graphite crucibles under vacuum or inert gas are preferred to minimize impurity formation. Induction heating provides a high-power outlet under a protective atmosphere. Therefore, it is preferred chiefly instead of commercial electrical furnaces, providing a relatively lower temperature for reactions.<sup>[60]</sup> Hot-pressing is a high pressure, high temperature, low strain rate process that densifies powder within graphite mold. In contrast to HP, heat generation is internal in SPS with pulsed current directly passing through the graphite die.<sup>[61]</sup> Joule heating provides higher densification, yielding densities comparable with the theoretical density of the compound. SPS has also been used for direct synthesis of borides (reactive SPS) such as  $\beta$ -boron<sup>[62]</sup> or  $AlMgB_{14}$ <sup>[63,64]</sup> and densification of powders before transport properties measurements.<sup>[65]</sup>

#### 2.1.3. Borothermal Reduction Method

Metal oxides and boron itself<sup>[37,66]</sup> or a boron source (e.g.,  $B_4C$ )<sup>[67,68]</sup> are mixed and heated to obtain  $MB_n$ . By the borothermal synthesis method, production on large scales and cost-effectiveness can be obtained with moderate-quality products. With an additional ball milling step, submicron particle size can be obtained.  $REB_n$  can also be synthesized by this method.

Hexaborides,<sup>[69]</sup>  $REB_{60}$ ,<sup>[37]</sup> borocarbonitrides<sup>[70,71]</sup> are generally synthesized by the borothermal method, according to the following generalized chemical reactions:



#### 2.1.4. Flux Method

As in the role of flux for crystal growth, a relatively high amount of a low-melting-point element (e.g., Al, Cu, Sn, Pb, In) is mixed with raw synthesis materials in a suitable crucible under a protective environment.<sup>[34]</sup> The flux method provides a liquid environment; thus, it decreases reaction temperature. After cooling, flux material is removed by an acid or alkali leaching, thus leaving the crystals as a solid residue. The flux growth mechanism is especially versatile to synthesize high-quality and large single crystals of  $B_{12}P_2$  and  $B_{12}As_2$  by using elemental boron as the source and nickel as the flux.<sup>[72]</sup>

#### 2.1.5. Molten Salt Electrolysis Method

The molten salt electrolysis method provides the reaction of borides at relatively lower temperatures by applying current density.<sup>[73]</sup> Electrochemical cells contain suitable cathode and anode with generally fluoride or chloride electrolytes and a reference electrode. The experiment is held in a protective environment in which boron and metal are added into electrolyte in stoichiometric quantities. Deposition on the cathode surface is controlled by refining parameters such as temperature, current density, etc.<sup>[68]</sup> Although this method is not efficient in obtaining products on large scales, it is preferred to reduce relatively medium reaction temperatures of di- and tetra- borides.<sup>[74]</sup>

## 2.2. Single Crystal Synthesis Methods

To determine their physical properties, various crystal growth methods are preferred to synthesize single-crystalline borides. A schematic view of the most-preferred techniques is shown in **Figure 3**.

#### 2.2.1. Floating Zone (FZ) Crystal Growth Method

The floating zone method is a crucible-free method that provides a synthesis of high-quality and cm-long single crystals of borides. Radiofrequency creates a melting zone between a single crystal seed and a high-purity polycrystalline material above the floating zone. The floating zone moves along the rod to contact the melt drop, which is formed at the bottom of the polycrystalline feed rod due to the relative motion of the heating device. After

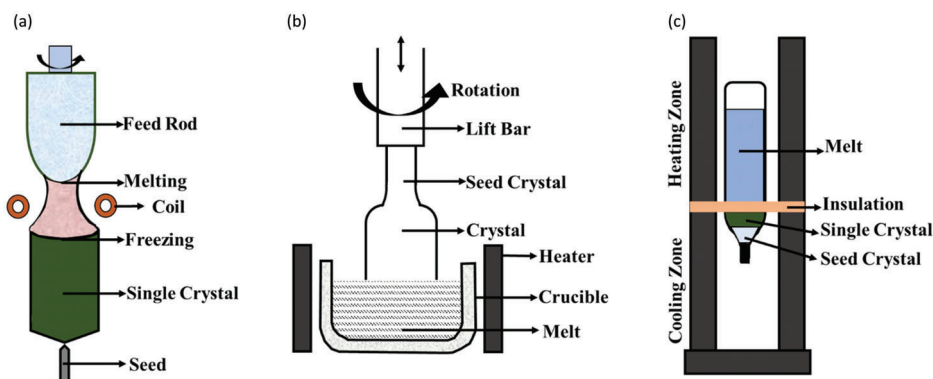


**Figure 3.** A schematic representation of single crystal growth techniques. a) Floating zone method; b) Czochralski method; c) Bridgman–Stockbarger method.

neck formation, dislocation-free molten material solidifies into a single crystal in limited dimensions due to the gravity effect on the liquid. The most common heating systems for the floating zone method include induction coil, resistance heater, optical heating (halogen lamps with mirrors). FZ method is one of the most employed techniques for growing single crystal of BCs<sup>[34,75]</sup> and REB<sub>50-60</sub>.<sup>[37,76,77]</sup>

### 2.2.2. Bridgman-Stockbarger Method

The Bridgman method is commonly used to grow a single crystal boule or ingot by temperature gradient and polycrystalline ingots if a seed crystal is not employed. Stockbarger method contains some additions such as high and low-temperature zones, or adiabatic loss zone. Therefore, these two methods are generally referred together in the literature. The polycrystalline material is melted thoroughly and then contacted with the single-crystal seed at the hot zone. Finally, the material is slowly cooled from one end of the container where the seed crystal is located.<sup>[78]</sup> This method has been used successfully to grow single crystals of YB<sub>66</sub><sup>[79]</sup> and AlFe<sub>2</sub>B<sub>2</sub><sup>[80]</sup> from the melt.

### 2.2.3. Czochralski Method

This method employs induction or resistance heating with cylindrical crucibles. After the feed material is wholly melted at temperatures slightly above its melting point, a seed crystal is dipped into the melt. Under rotation, the seed is slowly withdrawn from the melt; the feed melt crystallizes at the interface with a reduced temperature above its freezing point.<sup>[78]</sup> Transition metal diborides (for example, VB<sub>2</sub>,<sup>[81]</sup> TiB<sub>2</sub>, ZrB<sub>2</sub><sup>[82]</sup> and HfB<sub>2</sub>),<sup>[83]</sup> rare earth tetraborides (for example, YB<sub>4</sub>, TbB<sub>4</sub>, ErB<sub>4</sub>)<sup>[84]</sup> and Ni<sub>3</sub>B<sup>[85]</sup> are few examples in which the single crystals have been grown with this method.

## 2.3. Thin Film Synthesis Methods

### 2.3.1. Chemical Vapor Deposition Method (CVD)

The CVD method controls thin films' formation with chemical reactions; hence, it is more versatile than traditional methods.

In a typical CVD, the substrate is heated and exposed to volatile precursors that react on the surface. Heated substrate thermally activates a chemical reaction with a flowing precursor gas in the chamber, resulting in a uniform deposition. By-products and unreacted precursor gases are exhausted from the chamber.<sup>[86]</sup> Some of the B<sub>12</sub>P<sub>2</sub><sup>[87]</sup> and B<sub>12</sub>As<sub>2</sub><sup>[88]</sup> articles mentioned in this review have employed the CVD technique to obtain homogeneous thin films.

### 2.3.2. Ion Beam Evaporation Method

An intense pulsed ion beam is used to sputter a target, transforming the beam into thermal energy on the surface. Produced high-density ablation plasma is deposited on the substrate surface and produces thin films.<sup>[41,86]</sup> Since ions have equal energies, this method provides homogeneously distributed formation for thin films. Boron carbide thin films<sup>[41,89]</sup> in this review have been synthesized by the ion beam evaporation method.

## 3. Families of Known Borides

### 3.1. Di-, Tetra-, Hexa- Borides

#### 3.1.1. Diborides

Diborides are comprised of metal atoms sandwiched between 2D boron layers, as illustrated in **Figure 4**. The layered crystal structure determines the thermal and electrical properties such that the metal in the center provides electronic stability.<sup>[2,90]</sup> Diborides have attracted significant attention as superconductors (MgB<sub>2</sub>) or dopants.<sup>[90–92]</sup> However, they are poor thermoelectric materials due to their very low *S* and  $\sigma$  along with high  $\kappa$ . A study on 10 wt% PVA (polyvinyl alcohol) added TiB<sub>2</sub> reports a *zT* of 0.06 at 550 K.<sup>[90]</sup> Computational studies validated by experimental measurements revealed a metallic nature with *S* ranging from  $-2$  to  $+8 \mu\text{V K}^{-1}$  with the lowest thermal conductivity of  $51.9 \text{ W mK}^{-1}$ .<sup>[93–96]</sup> Doping studies are promising, considering that reduction in the thermal conductivity from 100 to  $30 \text{ mW K}^{-1}$  was achieved by incorporating SiC into TiB<sub>2</sub>.

On the other hand, diborides are pretty effective as dopants.<sup>[97]</sup> An interesting study reveals that the lattice thermal conductivity

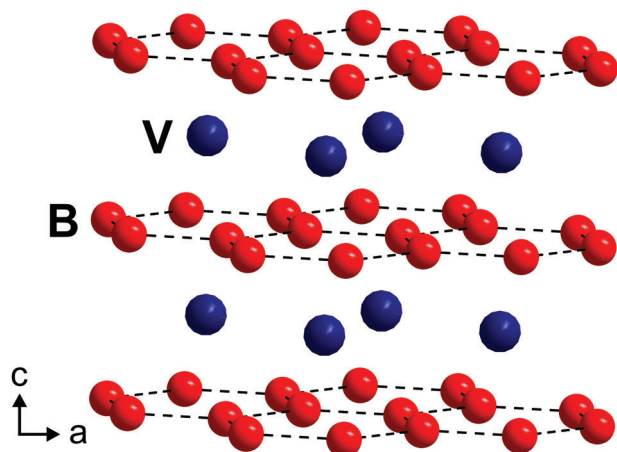


Figure 4.  $VB_2$  structure as a representative of  $AlB_2$  structure type.

( $\kappa_1$ ) of  $ZrB_2$ -SiC composites is strongly reduced at high temperatures. In such a case,  $ZrB_2$ -SiC composites attain high power factors,  $PFs > 1 \text{ mW mK}^{-2}$ , despite their metallic nature.<sup>[39]</sup> Similarly,  $HfB_2$  addition into  $B_{13}C_2$  reduces the density, resulting in lower  $\kappa$ . The metallic nature increases the charge carrier density of  $B_{13}C_2$ - $HfB_2$  composite, resulting in improved  $zT$  values.<sup>[98]</sup> High  $\sigma$  of  $TiB_2$  has also been found to increase the  $zT$  of  $PbSe$  and  $HfB_2$  to  $5 \times 10^{-4}$  and 0.12, respectively.<sup>[90,92,99]</sup> For  $FeSi$  and  $ZnO$ , the increase in the thermoelectric efficiency has been reported to be linearly dependent on the  $TiB_2$  concentration.<sup>[92]</sup> Despite being poor thermoelectric materials, diborides can be considered as promising dopants due to their metallic and refractory nature.

### 3.1.2. Tetraborides

Tetraborides have a 3D boron skeleton in which the electron-donating metal atoms stabilize the electron-deficient boron sublattice.<sup>[100–102]</sup> Classified as  $MB_4$  (M is mostly rare-earth or transition metals) or  $REMB_4$ , tetraborides embrace nearly all the rare-earth metals inside their 3D crystal structure.<sup>[103]</sup> Tetraborides have been extensively studied for magnetism and superhardness.<sup>[104–106]</sup>

$REB_4$  compounds are metallic because one of their three valence electrons ( $RE^{3+}$ ) resides in the conduction band.<sup>[103,107]</sup> However, only  $MgB_4$  has a bandgap of 1.6 eV, showing n-type semiconducting behavior.<sup>[95]</sup> Since metallic compounds such as  $UB_4$ ,  $CrB_4$ , and  $MnB_4$  have relatively high carrier concentrations resulting in low  $S$ , they have been reported to be poor thermoelectrics.<sup>[105,108–111]</sup> An interesting experimental study has uncovered the semi-metallic character of  $UB_4$ , which can be enhanced by utilizing  $^{11}B$ . Hence, an increase in the power factor to  $7.2 \times 10^{-4} \text{ Wm}^{-1} \text{ K}^{-2}$  has been achieved for  $U^{11}B_4$  at 850 K.<sup>[112]</sup> This value is two times larger than the PF of natural boron-containing  $UB_4$  and even higher than some boron carbide and  $\alpha$ - $AlB_2$  compounds. Such an increase has been attributed to introducing the impurities that optimize the carrier concentrations.

Ternary tetraborides,  $REMB_4$  (RE: Y, Gd, Ho; M: Transition metals such as Cr, Mo, W) are classified as  $ThMoB_4$ -type and  $YCrB_4$ -type, in which the latter is the most common.<sup>[112,113]</sup> As illustrated in Figure 5, these compounds are characterized by

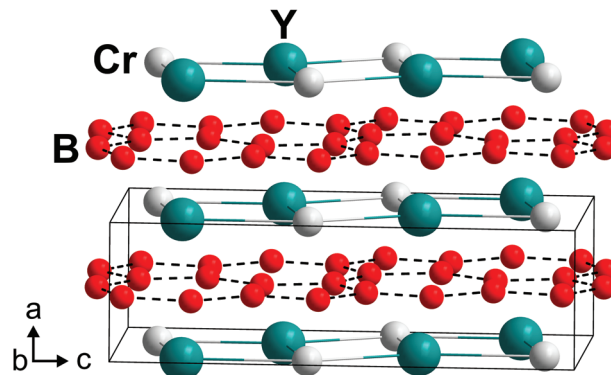


Figure 5. The crystal structure of  $YCrB_4$ , representative of tetraborides.

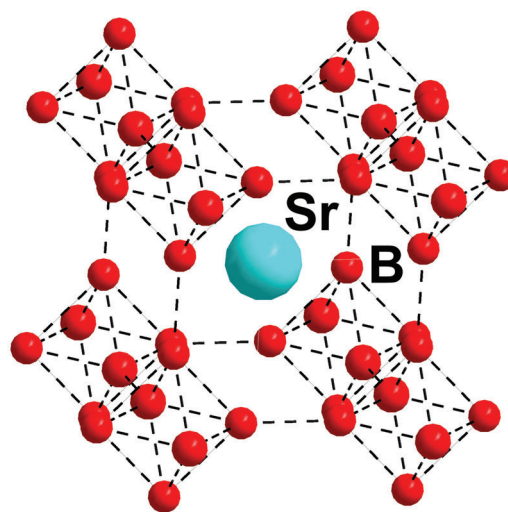


Figure 6. The crystal structure of  $SrB_6$ , representative of hexaborides.

three-bonded boron atoms making up 2D layers of five- and seven-membered alternating planar rings.<sup>[113–116]</sup>  $REMB_4$  materials are n-type semiconductors, which is an interesting feature due to the lack of n-type borides compared to their p-type counterparts.<sup>[57,117]</sup> Despite having moderate  $S$  values ranging from  $-70$  to  $-115 \text{ } \mu\text{V K}^{-1}$ , their low PF limits their use as TE materials. Thanks to the narrow bandgap of  $REMB_4$  compounds, the substitution of Fe for B yields a two-fold enhancement in PF in  $YMoB_4$ .<sup>[57]</sup> However, the obtained value of  $2.4 \text{ } \mu\text{W cmK}^{-2}$  is still far below those achieved in state-of-art TE materials, calling for further optimization.<sup>[57]</sup> A recent study on  $Y_{1-x}Ce_xCrB_4$  has obtained a  $zT$  of 0.06 at 800 K. Although too low for practical applications, this outcome widens the borides' application temperature (900–1700 K) and surpasses prior results reported for other borides such as  $CoB_{105}$ ,  $B_6O$ , or  $YB_{66}$ .<sup>[45,77,118,119]</sup>

### 3.1.3. Hexaborides

Hexaborides,  $MB_6$ , have a CsCl-type cubic structure in which  $B_6$  octahedra are located at the corners of the cube and surround the metal atom in the center.<sup>[38,117,120]</sup> A representative crystal structure for hexaborides is shown in Figure 6. The smallest rare earth metals do not form hexaborides, and stabilization of

these compounds gets trickier when the average size of the rare earth decreases.<sup>[103]</sup> Electronic conduction characteristics of hexaborides differ according to the valence state of the metal atom. Divalent ( $M = \text{Ba, Ca, Sr, Eu, and Yb}$ ) and trivalent hexaborides ( $M = \text{La, Gd, Dy}$ ) show semiconducting and metallic conduction behavior, respectively.<sup>[6,38,121]</sup> Mixed-valent hexaborides such as  $\text{SmB}_6$  ( $M = \text{Sm, Ce, Nd}$ ) exhibit a more complex electrical conduction behavior, which is still yet to be fully understood.

Most of the TE research on hexaborides has been focused on the divalent hexaborides since they possess high  $S$  and  $\sigma$ , whereas trivalent and mixed-valent ones possess small  $S$  due to their metallic nature.<sup>[122,123]</sup> Especially, alkaline-earth hexaborides are promising as n-type analogs of p-type TE borides.<sup>[124]</sup> The continuing interest in AEB<sub>6</sub> ( $\text{AE} = \text{Ca, Sr, Ba}$ ) derives from the donor defects in those structures, probably owing to cation vacancies or unintended impurities. The effect is that the electron concentration and mobility in the AEB<sub>6</sub> structures vary weakly in temperature and pressure.<sup>[125]</sup> Studies show that AEB<sub>6</sub> has similar negative  $S$  and  $\sigma$  for various AE elements.<sup>[126–128]</sup> The highest PF with a  $zT$  of 0.3 was obtained for  $\text{SrB}_6$ , which is the highest value obtained among divalent hexaborides studied hitherto.<sup>[129]</sup> Following those studies, a similar  $zT$  value of 0.3 has been also achieved in  $\text{CaB}_6$ ,<sup>[126]</sup> corresponding to a threefold increase with respect to prior work.<sup>[65]</sup>

There are still some concerns about the high  $\kappa$  of divalent hexaborides, which spans the range 10–40  $\text{W mK}^{-1}$ . As an alternative strategy to lower  $\kappa_{\text{lat}}$ , the production of thin films was investigated.<sup>[130,131]</sup> For high-temperature applications, the formation of solid solutions was studied to obtain ternary hexaborides with lower  $\kappa_{\text{lat}}$  because of their similar lattice parameters.<sup>[132]</sup> For the mixed crystals of  $\text{SrB}_6$ ,  $\text{CaB}_6$ , and  $\text{BaB}_6$ ,  $\kappa_{\text{lat}}$  was effectively reduced without significantly decreasing the electrical properties. For the compositions of  $\text{Ca}_{0.25}\text{Ba}_{0.75}\text{B}_6$  and  $\text{Ca}_{0.25}\text{Sr}_{0.75}\text{B}_6$ ,  $zT$  values of 0.2 and 0.25, respectively, were obtained at 1073 K.<sup>[126]</sup>  $zT$  around 0.35 was obtained in  $\text{Ca}_{0.5}\text{Sr}_{0.5}\text{B}_6$ , which is the highest value reported so far for n-type boron-rich solids.<sup>[127,128]</sup> In the same principle, the substitution of Yb for Ca in  $\text{CaB}_6$  lowered  $\kappa_{\text{lat}}$  by 20% while maintaining the high negative  $S$  values around 200–300  $\mu\text{V K}^{-1}$ .<sup>[66]</sup>

P-type hexaborides with large positive  $S$  also exist and an increase in  $S$  with increasing temperature due to the hopping conduction has been reported. A study on p-type  $\text{SiB}_6$  revealed an  $S$  value of 900  $\mu\text{V K}^{-1}$  at 1100 K, yielding a  $zT$  of 0.2.<sup>[58]</sup> For p-type  $\text{B}_6\text{O}$ , twice as much of  $S$  and similar  $zT$  around  $0.62 \times 10^{-3}$  at 1000 K were achieved compared with BC.<sup>[119]</sup> In the case of  $\text{YbB}_6$ , positive  $S$  was observed as high as those of AEB<sub>6</sub> up to 800 K, but thermal excitation of n-type carriers turned it negative.<sup>[133]</sup> Thus,  $\text{YbB}_6$  may be a p-type counterpart to n-type hexaborides. Similarly,  $\text{SrB}_6$  arises as an n-type counterpart of BCs.

## 3.2. Higher Borides

### 3.2.1. Dodecaborides

Icosahedral boron, or dodecaboron, forms the common unit cell of many thermoelectric borides such as  $\alpha$ - and  $\beta$ -rhombohedral polymorphs, BC,  $\text{YAl}_x\text{B}_{14}$ , and  $\text{YB}_{66}$ .<sup>[134]</sup> Except for the smallest  $\alpha$ -boron, all dodecaborides are promising thermoelectric materi-

als due to their high thermal and mechanical stabilities and scalable electronic properties.<sup>[135]</sup> The mechanical and thermal properties depend on the combination of various bonding types such as ionic, covalent, and metallic. Unique hybridization between the d orbitals of metals and p orbitals of boron is responsible for their enhanced transport and mechanical properties.<sup>[136]</sup>

The scalability of electronic properties results in a variety of dodecaborides formed by filling the electron deficiency in the crystal structure. The most suitable elements for this purpose come from groups 15 and 16 in the periodic table, such as  $\text{B}_{12}\text{As}_2$ ,  $\text{B}_{12}\text{S}_2$ ,  $\text{B}_{12}\text{P}_2$ , and  $\text{B}_{12}\text{N}_2$ .<sup>[137]</sup> Applying different synthesis routes or adding other impurity atoms enhances the electrical conductivity ( $\sigma$ ) and Seebeck coefficient of these compounds. For instance, despite the wide electronic band gap of  $\text{B}_{12}\text{As}_2$ , its electrical resistivity could be reduced by doping with Si.<sup>[137]</sup>

The single-crystal synthesis is an effective strategy to improve transport properties as well. Compared to polycrystalline  $\text{B}_{12}\text{As}_2$ , the single crystalline version was reported to have higher thermal conductivity (120–27  $\text{W mK}^{-1}$ ) due to the limited number of grain boundaries.<sup>[117]</sup> In the same study, electrical transport properties were also enhanced by annealing.<sup>[117,120]</sup> Although  $\text{B}_{12}\text{P}_2$  is a less toxic alternative to  $\text{B}_{12}\text{As}_2$ , it has a higher thermal conductivity value.<sup>[138]</sup> Doping with Si with the composition  $\text{B}_{12}(\text{Si})_x(\text{P}_2)_{1-x}$  further increases thermal conductivity and lowers  $zT$ .<sup>[72,88]</sup> Doping S into  $\text{B}_{12}$  seems to reduce resistivity, but the optimum dopant concentration has not been found yet.

$\text{AlMgB}_{14}$  has an orthorhombic crystal structure enabling doping of intrinsic vacancies to switch the p-type electrical conduction to n-type with Seebeck coefficients varying between +600 and –600  $\mu\text{V K}^{-1}$ . Co and Ni are effective dopants for this purpose, both of which enhance electrical conductivity as well.<sup>[139,140]</sup> Density of states (DOS) calculations also reveal that increasing the number of electrons exchanged between the metal and boron atoms enhances electrical properties.<sup>[63]</sup> On the other hand,  $\text{MgAl}_2\text{O}_4$  and  $\text{BO}_2$  can form during the synthesis of undoped  $\text{AlMgB}_{14}$ .<sup>[64]</sup> Since impurities influence electrical properties, powder mixture ratios of starting materials need to be controlled.<sup>[64]</sup> An interesting feature of  $\text{AlMgB}_{14}$  is that although  $\sigma$  and  $S$  are in between those of  $\beta$ -rhombohedral boron and boron carbides, its PF is the lowest.<sup>[141]</sup> Since  $\text{YB}_{14}$  have the same crystal structure as  $\text{AlMgB}_{14}$ , different techniques were applied to change the conduction behavior of  $\text{YB}_{14}$  to create n-type semiconductors. Because of the lower absolute values of the Seebeck coefficient and high thermal conductivities, the  $zT$  of the n-type counterpart is lowered than that of the p-type. Because the mechanical properties of  $\text{MB}_{14}$  compounds are superior to those of state-of-art thermoelectric materials, they are worth studying to enhance thermoelectric performance.<sup>[122,142,143]</sup>

Computational studies help reveal some new environmentally-friendly icosahedral borides like  $\text{ZrB}_{12}$ ,  $\text{HoB}_{12}$ ,  $\text{ErB}_{12}$ ,  $\text{TmB}_{12}$ , and  $\text{LuB}_{12}$ . Although these are generally superconductors, the unique crystal structure allows for modifications of their electronic properties.<sup>[107,115,116]</sup> The crystal structure of this compound can be thought of as a representative of dodecaborides. Here, the structure is composed of 8  $\text{B}_{12}$  icosahedra located at the edges and 2  $\text{B}_{12}$  icosahedra at the faces of the unit cell. Because of the 1/8 contribution coming from edges and 1/2 from the faces, the unit cell holds two complete  $\text{B}_{12}$  icosahedra. For clarity, these atoms are invisible in **Figure 7a**, and a  $\text{B}_{12}$  icosahedron

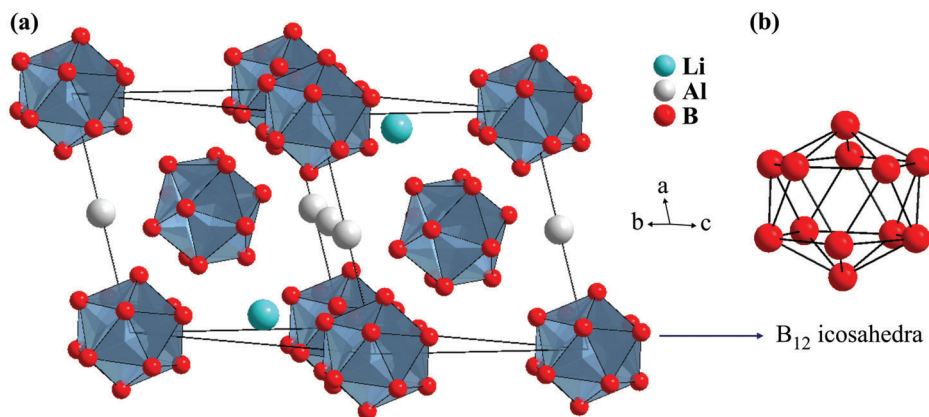


**Figure 7.** a)  $\text{LiAlB}_{14}$ , representative for dodecaborides. b) A schematic showing  $\text{B}_{12}$  icosahedra.

is shown in Figure 7b. There are 4 B atoms separate from the  $\text{B}_{12}$  icosahedra. On the other hand, 4 Al atoms are shared by 4 unit cells, and 1 Al atom is totally inside the unit cell resulting in 2 complete Al atoms. Finally, 2 Li atoms are located inside the unit cell. 2Li, 2Al, 4B, and  $2\text{B}_{12}$  icosahedra can be considered as  $\text{AlLi}(\text{B}_{12})\text{B}_2$ , that is,  $\text{AlLiB}_{14}$ .

Since  $\text{B}_{12}$  is ordered as layers in which metals can be inserted to donate electrons,  $\text{AlLiB}_{14}$  has been studied as a possible thermoelectric material. Experimental studies revealed a  $zT$  value of 0.5 at 1000 K, in agreement with the predictions of Density Functional Theory (DFT) calculations.<sup>[144]</sup> Considering the low  $\kappa$  and high mechanical properties of icosahedral borides, they are attractive for future research.

### 3.2.2. Boron Carbides

Boron carbides (BC) have outstanding refractory, mechanical, and chemical properties enabling applications in a wide range of areas, such as reactor technologies and thermoelectric power generation.<sup>[145]</sup> Similar to other boron-containing compounds, boron carbides have a low density ( $2.52 \text{ g cm}^{-3}$ ), high melting point ( $T_m > 2700 \text{ K}$ ), along with high mechanical hardness between 30 and 38 GPa.<sup>[40,145]</sup> The crystal structure of boron carbides is complex. The arrangement of C and B atoms changes depending on the chemical composition. A representative structure with a rhombohedral unit cell described in the  $R\bar{3}m$  space group (No. 166) is shown in Figure 7.<sup>[145]</sup> Although a hypothetical structure consists of  $\text{B}_{11}\text{C}$  icosahedra and C-B-C chains with a composition of  $\text{B}_{12}\text{C}_3$ , the actual structure comprises  $\text{B}_{12}$ ,  $\text{B}_{11}\text{C}$ , C-B-C, C-B-B, and C-vacancy-C chains.<sup>[137]</sup> BCs have a wide homogeneity range from B-rich to C-rich. Nevertheless, B-rich compounds are more stable and appropriate for thermoelectricity due to their lower  $\kappa$  values.<sup>[40,65,137,146–148]</sup> For this reason, we will hereafter provide a more detailed discussion on B-rich BCs while only a brief summary will be given on C-rich compounds.

BCs near the B saturation limit have higher mobility and carrier concentration than other boride-based compounds.<sup>[41]</sup> Moreover,  $\kappa$  decreases with increasing B content, and for a fixed B content, decreases with increasing temperature, making these compounds appropriate for high-temperature applications.<sup>[36,75,124,149]</sup> A high concentration of valence electron deficiencies results

in a prediction of metallic character for BCs; however, experimental studies reveal a p-type semiconducting nature with a high Seebeck coefficient of  $300 \mu\text{V K}^{-1}$ .<sup>[124]</sup> Attaining such a high value in a non-toxic compound attracted scientists to explore the electronic conduction mechanism of boron carbides, and two mechanisms were proposed:<sup>[93,150]</sup> Thermally activated small bipolaron hopping conduction, and combination of hopping between localized states and thermally activated band conduction.<sup>[124,137]</sup> The former is explained by assuming the presence of pairs of holes as the charge carriers that move by thermally-activated, phonon-assisted hops between electronic states of  $\text{B}_{11}\text{C}$  icosahedra.<sup>[124,137,150]</sup> The observed increase in the electrical conductivity with temperature supports this idea.<sup>[151,152]</sup> On the other hand, the latter disproves the former by experimentally showing that the high concentrations of gap states in the valence band result in p-type conduction and low electrical conductivity.<sup>[137]</sup> Studies conducted by Sauerschnig et al. were found to be consistent with this mechanism and reported  $S$  between  $225\text{--}280 \mu\text{V K}^{-1}$  along with a  $zT$  of  $0.027\text{--}0.046$  at  $973 \text{ K}$  for B-rich BCs.<sup>[149]</sup>

C behaves as an electron donor for BCs near the C saturation limit to compensate for the electron deficiency and lower the electrical conductivity. Thin-films of those materials were found to have a higher Seebeck coefficient and power factor. Various studies found the C content with the minimum Seebeck coefficient as  $\approx 13\%$ .<sup>[137,147]</sup> Further studies also revealed that the B/C ratio is essential in optimizing grain boundary barrier height to obtain larger grains with a large electrical conductivity. However, such materials have deteriorated Seebeck coefficient values resulting in a lowered power factor.

Thermoelectric properties of B-rich BCs can be further improved by doping with various elements or compounds like Ni, Fe, Si, P,  $\text{TiB}_2$ ,  $\text{SiB}_4$ , or  $\text{HfB}_4$ .<sup>[153–156]</sup> The addition of Si with four valence electrons increases the electrical conductivity and the Seebeck coefficient, resulting in a  $zT$  value of 0.15 at  $1500 \text{ K}$  ( $Z$  of  $1 \times 10^{-4} \text{ K}^{-1}$ ).<sup>[153]</sup> Nevertheless, P insertion reduces the hole concentration, giving rise to lowered electrical conductivity.<sup>[154]</sup> This study aimed to synthesize an n-type material, which could be reached by inserting 25.4 vol%  $\text{TiB}_2$  into  $\text{B}_4\text{C}$ .<sup>[157]</sup> The conduction mechanism shifted from small bipolaron hopping to electronic transport for this system, and  $\kappa$  was reduced by one-half of the undoped sample. One of the highest  $zT$  values of 0.29 at  $1100$

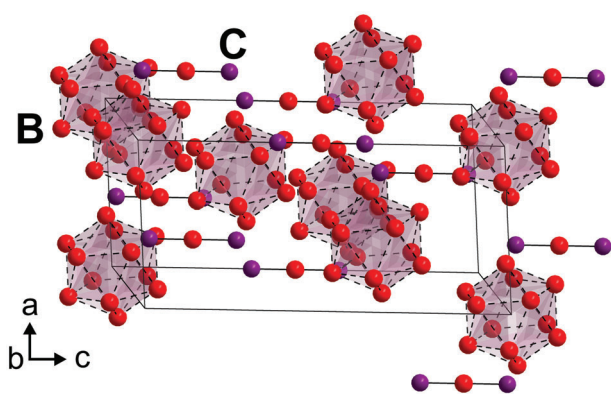


**Figure 8.** The crystal structure of  $B_{13}C_2$ , a representative of boron carbides.

$\kappa$  was found in  $SiC/B_4C$  composite. This relatively high value was attributed to the high Seebeck coefficient reaching up to  $400 \mu V K^{-1}$ .<sup>[158]</sup> Feng et al. reported that  $B_4C$ -Si-B composites consolidated by SPS exhibit lower  $\kappa$  but reach a low  $zT$  value of 0.036 at 1000 K for the sample with 10 wt% Si and 5.6 wt% B. Qin et al. doped  $B_{13}C_2$  (Figure 8) with Fe and calculated a band gap of 0.51 eV, suggesting that the extended states of 3d band of Fe could increase the electrical conductivity.<sup>[155,159]</sup> Fan et al. reported by DFT calculations that when Ni preferentially substitutes the C atoms in BC at the end of the C-B-C chain instead of the B atoms. The weaker Ni-B covalent bond decreases  $\kappa$ .<sup>[156]</sup> Innocent et al. reported  $HfB_2/BC$  (13.3 at% C) composite with optimum  $HfB_2$  content of 10 wt% with a peak  $zT$  of 0.20 at 1000 K.  $HfB_2$  addition reduces  $\kappa$ ; however, since  $HfB_2$  is a poor sintering additive leading to a lower density, no significant improvement in the thermoelectric properties was observed. Since  $HfB_2$  is metallic, the  $S$  is reduced with increasing the  $HfB_2$  content.<sup>[98]</sup> Finally, Cai et al. reported higher  $\sigma$  and  $\kappa$  combined with lower  $S$  for  $W_2B_5/B_4C$  composite by hot-pressing. The  $zT$  is higher than that for  $B_4C$  and is about  $1.03 \times 10^{-4} K^{-1}$  at 1500 K.<sup>[160]</sup>

### 3.2.3. Borocarbonitrides (REBC(N))

In borocarbonitrides,  $B_6$  and  $B_{12}$  units are connected to C-B-C chains, while rare-earth atoms form layers, as shown in

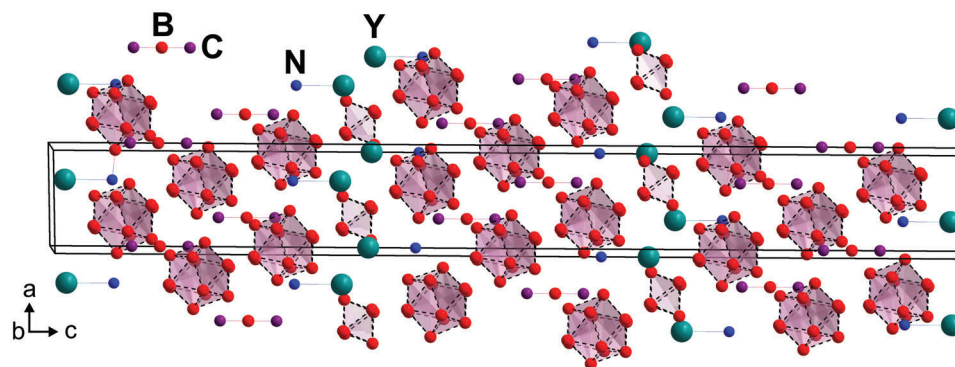


**Figure 9.** The crystal structure of  $YB_{22}C_2N$ , representative of borocarbonitrides.

**Figure 9.**<sup>[161,162]</sup> The  $B_{12}$  icosahedra and C-B-C chain layers rise in the order of  $REB_{17}CN$ ,  $REB_{22}C_2N$ , and  $REB_{28.5}C_4$ .<sup>[163]</sup> These compounds are homologous to  $B_4C$  with  $B_{12}$  icosahedra layers.<sup>[35,59,164]</sup> Multiple sintering routes can be followed to synthesize them in phase-pure polycrystalline form. Nevertheless, the densification processes (pressing and then annealing) are only successful up to 50% of the theoretical density, which influences the results quite significantly.<sup>[164]</sup>

$REB_{22}C_2N$  (RE: Y, Er, Lu) and  $HoB_{17}CN$  samples are the first examples of unmodified boron-rich compounds showing n-type conduction.<sup>[165]</sup> Compared to other well-known borides, their  $\rho$  was higher, and their  $\kappa$  was lower due to their low relative density. The comparison of the  $\kappa$  values of these compounds, which possess relatively low but similar densities, shows that  $HoB_{17}CN$  and  $ErB_{22}C_2N$  exhibit similar very low values of around  $1 W mK^{-1}$ . Both are lower than the  $\kappa$  values reported for  $YB_{28.5}C_4$ . These tend to be dependent on the homologous sequence with  $\kappa$  increasing as the number of boron cluster layers increases, suggesting that heavy rare-earth atoms in the light boron matrix may be a key ingredient to influence  $\kappa$ .<sup>[35]</sup>

SPS technique increased the relative density of  $YB_{22}C_2N$  up to 75% and even 95% with the addition of additives such as  $YB_4$  and  $YB_{25}C$ .<sup>[59,164]</sup> The addition of  $YB_{25}C$  increased the absolute value of  $S$  besides the densification improvement.<sup>[59]</sup> Even with the 75% relative density, grain growth induced by SPS led to lower  $\rho$  and slightly higher  $\kappa$ , which enhanced the  $zT$  value 12 times but led to a low peak value of  $2.5 \times 10^{-5}$  at 1000 K.<sup>[164]</sup> Later, REBC(N) compounds were found to have very large anisotropy in the  $\kappa$  values, which are low along the boron cluster layers along the c-axis but comparatively higher in the rare-earth layers.<sup>[70]</sup> Such a behavior may be used in future studies for controlling the microstructure of those materials and hence, tuning their thermoelectric efficiency.

In order to decrease the relatively high  $\rho$  of borocarbonitrides, metal borides or transition metals have been selected as dopants.  $ErB_4$  and  $ErB_6$  doping into  $ErB_{22}C_2N$  and  $ErB_{17}CN$  resulted in a significant reduction of  $\rho$  by up to two orders of magnitude. For the  $ErB_{22}C_2N:ErB_4$  sample, the increase in  $\kappa$  calculated to be close to 20% was outweighed by the reduction in  $\rho$ . Therefore, PF was successfully increased, and a  $zT$  of  $1.7 \times 10^{-5}$  was achieved at 1000 K.<sup>[163]</sup> Rh, Cu, Ni, Co doping in  $YB_{22}C_2N$  resulted in slightly lower negative  $S$  and lower  $\rho$  values, leading to an increase in PF by two orders of magnitude for the Co-doped sample.  $VB_2$

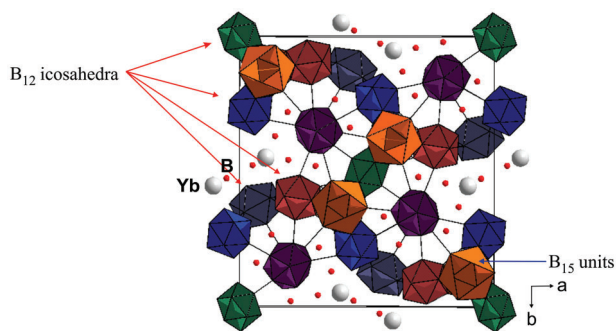


**Figure 10.** The crystal structure of  $\text{YB}_{43}$ , representative of rare-earth borides.

addition to  $\text{YB}_{22}\text{C}_2\text{N}$  decreased the  $\rho$  and showed  $S$  of  $-89 \mu\text{V K}^{-1}$ , whose absolute value is 2.2 times larger than that of the undoped  $\text{YB}_{22}\text{C}_2\text{N}$ .<sup>[99]</sup>

The p-type conduction in  $\text{YB}_{28.5}\text{C}_4$  was first explained by its metal-poor nature.<sup>[102]</sup> Later on, however,  $\text{YB}_{28.5}\text{C}_4$  samples were found to contain BC clusters, which switch the n-type conductivity into p-type.<sup>[165]</sup> Therefore, the negative  $S$  of the other REBC(N) compounds is relatively low in absolute values compared to other boron cluster compounds. The  $zT$  of the “pure”  $\text{YB}_{28.5}\text{C}_4$  samples was very low (below  $10^{-3}$ ), which again is due to the lack of high relative densities. Additionally, the  $S$  showed an increase in the absolute values upon decreasing the carbon content, which can be a promising route to boost negative  $S$ .<sup>[166]</sup>

Research on this family is quite important due to their n-type electrical conduction. Focusing on better densification methods while enhancing their relatively lower  $\sigma$  values by seeding/doping experiments might further increase the thermoelectric performance of these types of higher borides.

### 3.2.4. Rare Earth Borides ( $\text{REB}_{50}$ — $\text{REB}_{66}$ )

Rare-Earth Borides contain a rare-earth metal such as Yb, Y, Tb, Dy, Ho surrounded by  $\text{B}_{12}$  icosahedra along with  $\text{B}_{15}$  units.<sup>[167]</sup> A representative structure belonging to  $\text{YbB}_{43}$  is illustrated in **Figure 10**. Here,  $\text{B}_{12}$  units comprised of the same B atoms are shown with the same color, that is, there are five different  $\text{B}_{12}$  icosahedra. Furthermore,  $\text{REB}_{66}$ ,  $\text{REB}_{50}$ , and  $\text{REB}_{44}\text{Si}_2$  are other common examples of rare-earth borides having many similarities in their crystal structures.  $\text{REB}_{66}$  compounds have one of the most complex structures among all-known boron compounds with  $\approx 1600$  atoms in the unit cell resulting in extremely low, glass-like  $\kappa$ .<sup>[168]</sup> This is the reason why these compounds are considered as strong candidates for the well-known PGEC concept.<sup>[37]</sup>  $\text{REB}_{50}$  compounds have an orthorhombic crystal structure described in the  $P2_12_12$  space group with lattice constants similar to those of  $\gamma\text{-AlB}_{12}$ .<sup>[169]</sup> Isostructural families of  $\text{REB}_{50}$  such as  $\text{REB}_{44}\text{Si}_2$  crystallize in the Pbam space group.<sup>[169,170]</sup>

Glass-like  $\kappa$  values of  $\text{REB}_{66}$  are attributed to their crystal complexity, possible rattling phenomena of the RE atoms typically observed in cage-like compounds such as skutterudites or clathrates,<sup>[171,172]</sup> symmetry mismatch effect, or occupancy disorder in the structure.<sup>[173]</sup> On the other hand, large  $S$  values around  $800 \mu\text{V K}^{-1}$  were obtained for  $\text{SmB}_{66}$ ,  $\text{YB}_{66}$ ,  $\text{YbB}_{66}$ , and  $\text{ErB}_{66}$  at

room temperature. Although these values are higher than those of the best room-temperature TE materials  $\text{Bi}_2\text{Te}_3$ , the extremely large resistivity of  $\text{REB}_{66}$  compounds results in a very poor PF and  $zT$ . Indicative of degenerate semiconducting behavior, electrical resistivity, and Seebeck coefficient decrease with increasing temperature, resulting in a higher PF at high temperatures. For instance, a very recent study on  $\text{YbB}_{66}$  reported the  $zT$  to be 0.1 at 973 K.<sup>[174]</sup> Another study on  $\text{YB}_{66}$  and  $\text{ErB}_{66}$  gave rise to a  $zT$  of 0.13 at 1050 K, extrapolated to 0.4 at 1500 K.<sup>[37]</sup> For  $\text{YbB}_{66}$ , C doping reduced thermal conductivity and enhanced  $zT$  by about two orders of magnitude.<sup>[77]</sup> The  $\kappa$  values of  $\text{SmB}_{62}$  and  $\text{SmB}_{60}$  are even lower than that of  $\text{YB}_{66}$  due to the much larger molar mass of Sm. The mixed valency in the  $\text{REB}_{66}$  type compounds, which is assumed to be the main reason behind their enhanced  $\sigma$  while maintaining similar  $S$ , was first reported in the same study.

While boron-rich borosilicides,  $\text{REB}_{44}\text{Si}_2$ , have low  $\kappa$  and  $S$  values similar to  $\text{REB}_{66}$ , they have significantly higher electrical conductivity.<sup>[7]</sup>  $\text{REB}_{44}\text{Si}_2$  shows comparatively superior PF than  $\text{ErB}_{66}$  while maintaining a similar low  $\kappa$ , which is characteristic of rare-earth  $\text{B}_{12}$  icosahedral compounds.<sup>[170]</sup> The peak  $zT$  of 0.2 can be extrapolated for  $\text{REB}_{44}\text{Si}_2$  ( $\text{RE} = \text{Tb}, \text{Er}, \text{Tm}, \text{Yb}$ ), and doping yielded a 30% increase in the PF to reach  $1.2 \times 10^{-4} \text{ V}^2 \text{ K}^{-2} \Omega^{-1} \text{ m}^{-1}$  while improving the crystallinity.<sup>[7,71,166,175]</sup> Other transition metals such as Mn, Fe, Cu, Rh, Mo, and Ti decreased the  $\rho$  of  $\text{YB}_{44}\text{Si}_2$  but did not result in a net gain in  $zT$ . Among all doping elements, the addition of Mo and Ti readily resulted in the presence of their corresponding diborides.<sup>[140]</sup> As a result, it was suggested to utilize smaller concentrations of doping elements to enhance  $zT$ .<sup>[140]</sup> One interesting outcome is the negative  $S$  ( $-20 \mu\text{V K}^{-1}$ ) of Rh-doped  $\text{YB}_{44}\text{Si}_2$  regarding the need for n-type counterparts of boride-based thermoelectric materials.<sup>[175,176]</sup>

### 3.2.5. Betaboron

Boron has two allotropes referred to as  $\alpha$  and  $\beta$  in which the  $\alpha$ -allotrope is unstable and dissociates into  $\beta$ -boron at high temperatures. The peak  $zT$  of  $\beta$ -boron is obtained at high temperatures, so that it may be used at temperatures above 1700 K.<sup>[46,48]</sup> The rest of this review deals with  $\beta$ -boron and its possible thermoelectric applications.

The complicated crystal structure of  $\beta$ -boron  $[(\text{B}_{12})_4(\text{B}_{28})_2]\text{B}$  with 105 B atoms and five vacancy sites determines its thermoelectric and mechanical properties. The structure reported in **Figure 11** includes 8  $\text{B}_{12}$  icosahedra at the edges and 12 of them at the sides of the unit cell. The former is shared by 8 UCs, whereas the latter is shared by 4 UCs resulting in 4 complete  $\text{B}_{12}$  icosahedra. On the other hand, 2  $\text{B}_{28}$  units reside totally inside the unit cell. These units are formed by the fusion of 3  $\text{B}_{12}$  icosahedra in which three of them share one atom, and two icosahedra share two atoms. Each icosahedron has seven unshared atoms. In the structure of  $\text{B}_{105}$ , various elements can be inserted into vacancies to tune the electrical properties, and a summary chart is reported in **Table 1**. Results indicate that the nature of the doping element, its location, concentration, and remaining vacancies are critical in determining the electrical conductivity and the Seebeck coefficient of  $\beta$ -boron. Moreover, atoms tend to fill some specific vacancies depending on the size of the vacancy and the charge of the dopant.<sup>[46,177]</sup> For example, occupation of  $\text{A}_1$  sites is directly

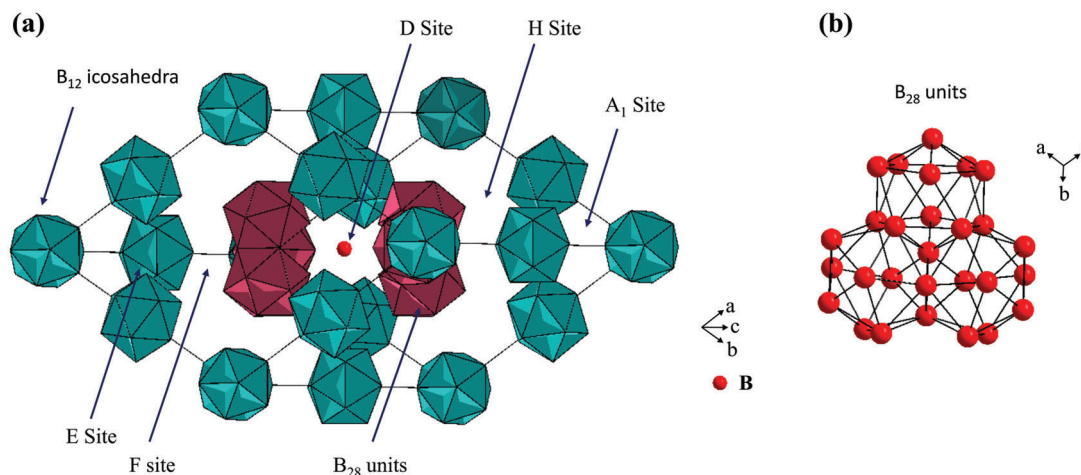


**Figure 11.** a) The crystal structure of  $\beta$  – boron, b) A detailed schematic of  $B_{28}$  units.

**Table 1.** Possible doping sites of  $\beta$ -rhombohedral boron with corresponding thermoelectric properties.

Doping element	Interstitial site	$S$ [ $\mu\text{V K}^{-1}$ ]	$\alpha$ [ $\Omega^{-1} \text{cm}^{-1}$ ]	$K$ [ $\text{W mK}^{-1}$ ]	Radius [pm]
Cu	$A_1, D, E$	200	13	2.1	140
Co	$A_1, E$	200	10	4	200
V	$A_1$	-450	-	6	205
Zr	$D, E$	-650	-	-	160
Fe	$A_1, D$	-350	-	-	126
Mg	$A_1, H, D, F, E$	-	10	-	173
Li	$F, E$	-	0.05	-	182
Mn/Sc/Zr	$D, E$	-	-	-	161/230/160
Cr/Al	$A_1, D$	-	-	-	200/184
Si	$A_1$	-	-	-	210

(Cu, Co, V, Mg, Li, Mn/Sc, Cr,<sup>[181]</sup> Al, Si;<sup>[46]</sup> Fe;<sup>[46,179]</sup> Zr<sup>[45]</sup>)

correlated with  $\sigma$ , while  $S$  is affected by the atoms in the D site. On the other hand, by comparing the variations in the electrical and thermal transport properties, the location of each atom can be determined. When  $\beta$ -rhombohedral boron was doped with transition metals such as Cr, Fe, Co, Ni, Cu,  $\sigma$  was increased, but  $S$  was decreased except for Zr doping. A summary of the variations in the transport properties induced by various elements is reported in Table 1.<sup>[44,47,137,178]</sup>

The electronic conduction of  $\beta$ -boron is determined by variable range hopping (VRH), which is indicated by increasing electrical conductivity and Seebeck coefficient with increasing temperature.<sup>[44,45]</sup> However, the hybridization of the holes in  $\beta$ -boron becomes significant when a transition metal is added. For instance, the  $\sigma$  of Fe-doped  $\beta$ -boron increases proportionally with the Fe concentration, whereas no such behavior is reported for Al doping.<sup>[179]</sup> It is worth noting that the  $A_1$  site should be filled in order to tune the electrical conductivity, and Al, Fe, Cu, and Cr are suitable for this purpose.<sup>[47]</sup> Solubility limits and coprecipitates have an important effect on electrical conductivity as well. When Cr is doped to the  $A_1$  site, the value of  $\sigma$  decreases with increasing Cr content because of the formation of a secondary phase that de-

creases the Cr concentration in the matrix. Moreover, in the case of doping W and V into  $\beta$ -B, the concurrent increase in  $\sigma$  and decrease in  $S$  were probably the result of the metallic character of the secondary phases  $WB_4$  and  $VB_2$ , or charge transfer from V to boron icosahedra.<sup>[47,62]</sup> Overall, the addition of Mo, Ru, and V resulted in  $MoB_4$ ,  $RuB_2$ ,  $VB_2$  as impurities. In all these samples, the lattice thermal conductivity values were nearly the same. Hence, the addition of  $VB_2$  yielded the second-highest  $zT$  values reported for all metal-doped  $\beta$ -rhombohedral boron materials with a value of  $7.91 \times 10^{-3}$  at 1079 K.<sup>[62]</sup>

Boron has a huge affinity for carbon, allowing a combination of interstitial and substitutional alloying to enhance the electrical conductivity.<sup>[178]</sup> Each boron icosahedra can accommodate two carbon atoms to form an interstitial alloy. Moreover, the boron atom in the center can be exchanged with a carbon atom, thereby forming a substitutional alloy. Considering that the maximum solubility of C into B is 9 C atoms per  $\beta$ -rhombohedral boron unit cell, the linear relationship between electrical conductivity and the amount of C can be expressed as<sup>[45,178,180]</sup>

$$\sigma = 1.2 \times 10^{-7-1} \text{ cm}^{-1} + (1.1 \times 10^{-6-1} \text{ cm}^{-1})/\text{at\% C} \quad (6)$$

This formula results in reasonable room temperature electrical conductivity which is invalid for concentrations higher than 1.1 at%. Between 900 and 1000 K, the electrical conductivity of 8.5 at% C doped  $\beta$ -boron was found to be  $0.04 \text{ ohm}^{-1} \text{ cm}^{-1}$  with a corresponding  $zT$  of 0.01.<sup>[178]</sup>

The reason behind the moderate  $zT$  values is the high  $S$  ( $950 \mu\text{V K}^{-1}$ ) of  $\beta$ -boron compounds, indicating p-type character.<sup>[47,177]</sup> Seebeck coefficient can be either changed from negative to positive, or its absolute value can be increased by doping.<sup>[46]</sup> Since Cr and Fe occupy  $A_1$  and D sites, they can be both doped to form  $Cr_{0.8}Fe_{0.2}B_{105}$  with enhanced Seebeck coefficient. Moreover,  $CrB_{105}$  is n-type, which is promising for thermoelectric applications. Interestingly,  $VB_{105}$  is n-type only if the concentration is 0.24 at%. When Zr is used as the doping element, however,  $S$  continuously decreases from 400 to  $-670 \mu\text{V K}^{-1}$  so that the semi-conducting behavior changes from p-type to n-type with the most negative value reported for metal-doped samples. This property

is characteristic of  $\beta$ -boron compounds because of its intrinsic semiconducting behavior dominant at high temperatures.<sup>[69]</sup>

The thermal conductivity of  $\beta$ -rhombohedral boron is around  $8 \text{ W m}^{-1} \text{ K}^{-1}$  at 1000 K, which is slightly higher than many state-of-art thermoelectric materials. Due to interstitial vacancies in the structure, phonon scattering can be increased to decrease the lattice's thermal conductivity. Separate studies in which Hf, Co, Zr, Sr, W, or Cu were used as doping elements support this idea.<sup>[45]</sup> Among those, Cu inserted into D and E sites effectively reduced the thermal conductivity and resulted in a peak  $zT$  of 0.038. The application of different synthetic routes is also effective in reducing thermal conductivity. For instance, doping of Co by arc melting rather than hot press results in a lower  $\kappa$  and higher  $zT$ .<sup>[181]</sup>

For practical applications of thermoelectric materials, hardness is an essential criterion in which  $\beta$ -rhombohedral boron is attractive with a microhardness value of 32 GPa. Considering the vacancies, hardness can be further increased by forming new bonds with guest atoms and boron.<sup>[7]</sup> A recent study reveals that the increasing concentration of dopants such as Al, Cu, Sc, Mn, Mg, and Li increases the mechanical properties of  $\beta$ -boron significantly up to 43 GPa.<sup>[7]</sup> Due to their mechanical stability and tunable thermoelectric transport properties,  $\beta$ -rhombohedral borides might be a promising family for future thermoelectric applications.

#### 4. Boron and Borides Incorporation into Thermoelectric Materials

Due to its non-toxicity, abundance, and low atomic radius, nano-boron is a promising dopant, especially for p-type semiconductors. In this respect, when nano-boron was inserted into  $\text{Cu}_2\text{Se}$ , grain boundaries were accommodated by boron to reduce the lattice thermal conductivity and enhance  $zT$  up to 1.4 at X K.<sup>[52]</sup> Similarly, carbon-coated boron (C/B-NPs) inclusion into  $\text{Cu}_2\text{Se}$  also increased  $zT$  by 55%. Newly formed Cu:C:B interface here is responsible for the extremely low thermal conductivity of  $0.28 \text{ W m}^{-1} \text{ K}^{-1}$ .<sup>[53]</sup>  $\text{Bi}_{0.5}\text{Sb}_{1.5}\text{Te}_3$  is another promising material for nanostructuring. In this material, B precipitated into grain boundaries to reduce thermal conductivity without deteriorating electrical transport properties. As a result, a significantly high  $zT$  of 1.6 at 375 K was obtained.<sup>[182]</sup> The effect of boron on thermoelectric properties can change depending on whether the material is single-crystalline (SC) or polycrystalline (PC). Although the  $zT$  of B-doped SC  $\text{Mg}_2\text{Si}$  showed a sixfold increase, B doping did not change  $zT$  when the material was polycrystalline.<sup>[54,183]</sup>

$\text{TiB}_2$  is another excellent phase to incorporate a thermoelectric material because of its inherently large electrical conductivity.<sup>[97]</sup> For instance, the addition of  $\text{TiB}_2$  into  $\text{YB}_{22}\text{C}_2\text{N}$  and  $\text{PbSe}$  increased their  $zT$  up to  $5 \times 10^{-4}$  and 0.12, respectively.<sup>[90]</sup> In both cases, the increase in  $zT$  was found to result from an enhanced power factor.<sup>[99]</sup> Although  $zT$  of  $\text{TiB}_2$ -incorporated  $\text{ZnO}$  is smaller than that of  $\text{TiB}_2$ , it is higher than that of undoped  $\text{ZnO}$ . However, the improvement is concentration-dependent and obtained only if the  $\text{TiB}_2$  concentration is 10%.<sup>[92]</sup> Another concentration dependence was observed in the  $\text{TiB}_2$ - $\text{FeSi}$  system. Here, the best concentration was 5 vol%, with a corresponding  $Z$  of  $1.9 \times 10^{-4} (1/\text{K})$ .<sup>[92]</sup>

B doping can be applied to enhance the mechanical properties as well. It was found that  $\alpha\text{-MgAg}_{0.97}\text{Sb}_{0.99-x}\text{B}_x$  has a

higher thermal conductivity and a lowered  $zT$  compared to  $\text{MgAgSb}$ . However, the microhardness of this compound was increased from 282 to 396 Hv because of the strengthening induced by adding B.<sup>[184]</sup>

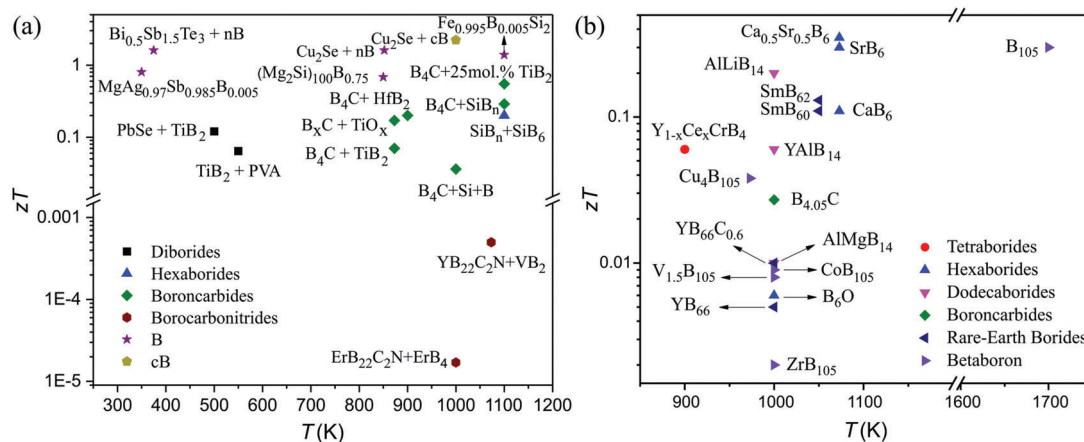
#### 5. Trends in Transport Properties and $zT$ Values

Figure 12a,b shows the dimensionless thermoelectric figure of merit  $zT$  as a function of temperature for various boron-doped and boron-based compounds. While in the latter ones, the  $zT$  values remain limited to around 0.4 above 1000 K, high thermoelectric performance could be achieved in thermoelectric compounds in which boron has been used as an additive element. Divalent hexaborides, for example,  $\text{CaB}_6$  and  $\text{SrB}_6$ , have shown promising thermoelectric properties due to their semimetal or small-gap semiconductor nature. Their somewhat large thermal conductivity can be lowered when they are fabricated as films, which may make them less suitable for large-scale thermoelectric applications. As it is apparent in Figure 12b, nano-boron or carbon-coated nano-boron is a promising dopant for p-type thermoelectric materials. When incorporated into materials such as  $\text{Cu}_2\text{Se}$  and  $\text{Bi}_{0.5}\text{Sb}_{1.5}\text{Te}_3$ , boron can tune the electronic transport properties by doping and reduce the lattice thermal conductivity through, for example, scattering of phonons through interfaces or multiscale hierarchical architectures, and thus, enhance the thermoelectric figure of merit dramatically.

The trend in the lattice thermal conductivity  $\kappa_L$  as a function of the unit cell volume (Figure 13) follows the basic expectation that increasing the number of atoms per primitive unit cell should tend to decrease  $\kappa_L$  due to the high number of low-velocity optical modes. Going from  $\text{B}_4\text{C}$  to  $\text{YB}_{66}$  through  $\beta$ -B results in a significant lowering of  $\kappa_L$  by two orders of magnitude, with the cage-like compound  $\text{YB}_{66}$  exhibiting glass-like  $\kappa_L$ . Although the microscopic mechanisms governing the thermal transport in many families of TE materials have been investigated in detail, little is known about the lattice dynamics of boron-based compounds. Future detailed studies of the low-energy region of the phonon spectrum by inelastic neutron and/or X-ray scattering will be helpful in determining the influence of the structural complexity on  $\kappa_L$ . In this regard, the possibility of growing large, high-quality single crystals opens up an essential experimental window through which the lattice dynamics of these compounds may be investigated in detail.

#### 6. Conclusion and Future Prospects

For extremely high-temperature applications in the range of 1000–2000 °C, such as in jet engine exhausts and fusion power generation, borides are among the few thermoelectric materials that can withstand these temperatures and have the potential to display relatively higher  $zT$  values than those reported in the literature so far. With the use of various synthesis techniques, boron-based compounds have been constantly discovered and investigated over the last decades. Due to the peculiar chemistry of elemental boron, most of these materials feature high structural complexity, culminating in the cage-like compounds  $\text{REB}_{66}$ . This complexity, which can be manipulated by varying the metallic elements, yields very low lattice thermal conductivity



**Figure 12.** Maximum achieved  $zT$  vs. Temperature (K) of a) some of boron and boron-based compounds;<sup>[37,45,62,65,66,91,118,119,128,136,143,149,165,181,185]</sup> b) doping studies of elemental boron or boron compounds into promising thermoelectric materials.<sup>[34,35,50,52,53,58,90,98,99,147,182–184,186–188]</sup> See **Tables A1** and **A2** in Appendix.

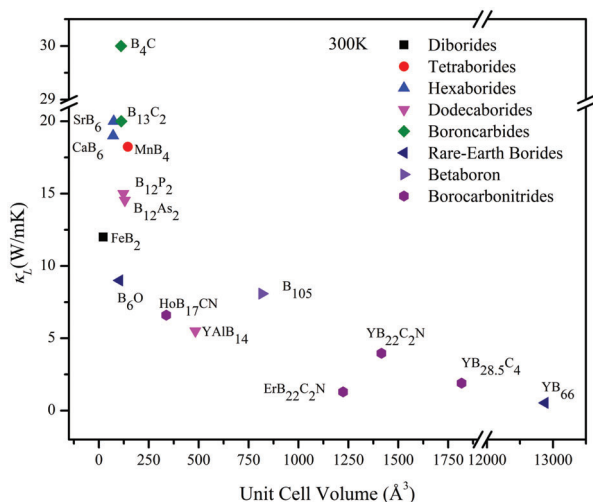


**Figure 13.** Unit cell volume ( $\text{\AA}^3$ ) vs lattice thermal conductivity,  $\kappa_L$  ( $\text{Wm}^{-1}\text{K}^{-1}$ ), of selected borides at 300 K.

approaching that of amorphous solids. This appealing characteristic, combined with high thermal and mechanical stability up to very high temperatures, is a prerequisite that makes these compounds a potential candidate for thermoelectric applications in power generation. Both n- and p-type electrical conduction could be achieved in several families of boron-based materials, opening up interesting prospects for integration in thermoelectric devices. Despite very high  $zT$  values have been obtained for boron-incorporated compounds, significant efforts need to be devoted to the optimization of the thermoelectric properties of pure boron-based compounds (the highest estimated  $zT$  value obtained so far remains limited to  $\approx 0.5$  at 1500 K). The lack of high-performing boron compounds is mainly tied to the rigid covalent network that often results in high sound velocities and hence, in high lattice thermal conductivity. Reducing the ability of these compounds to transport heat is an important challenge to overcome in future studies. In this regard, the search for cage-like compounds might be an interesting line of research to

pursue in addition to defect engineering and nanostructuring. A second challenge will be related to the identification of semiconducting boron compounds, which will help achieve higher thermoelectric performance than in metallic compounds. Extending the landscape of semiconducting materials would open up novel opportunities for using the full arsenal of strategies that have been particularly effective in optimizing the thermoelectric properties of chalcogenide semiconductors. Band-structure engineering tools such as band convergence or resonant levels provide mechanisms that can enhance the PF and that are yet to be investigated in boron compounds. Another important issue to be addressed in future studies is the lack of systematic measurements of the charge carrier concentration and mobility. These physical parameters are particularly important for developing structure/property relationships and guiding doping strategies. This will also help determine whether the structural complexity sought after for reducing heat transport can be achieved while maintaining high carrier mobilities. Looking further ahead to the future, the deployment of the full arsenal of synthesis techniques and sophisticated strategies developed in the past decades to optimize the thermoelectric properties may lead to the discovery of boron-based compounds with thermoelectric performance rivaling that of state-of-the-art thermoelectric materials.

## Appendix

**Table A1.** Materials represented in Figure 12a with corresponding reference numbers.

Material	Ref.	Material	Ref.	Material	Ref.
$\text{Y}_{1-x}\text{Ce}_x\text{CrB}_4$	[118]	$\text{AlLiB}_{14}$	[185]	$\text{YB}_{66}\text{C}_{0.6}$	[165]
$\text{SrB}_6$	[38]	$\text{YAlB}_{14}$	[143]	$\text{B}_{105}$	[62]
$\text{B}_6\text{O}$	[119]	$\text{B}_{4,05}\text{C}$	[149]	$\text{Co}_1\text{B}_{105}$	[45]
$\text{CaB}_6$	[66]	$\text{SmB}_{60}$	[37]	$\text{Cu}_4\text{B}_{105}$	[181]
$\text{Ca}_{0.5}\text{Sr}_{0.5}\text{B}_6$	[128]	$\text{SmB}_{62}$	[37]	$\text{V}_{1.5}\text{B}_{105}$	[45]
$\text{AlMgB}_{14}$	[65]	$\text{YB}_{66}$	[136]	$\text{Zr}_{1.0}\text{B}_{105}$	[91]

**Table A2.** Materials represented in Figure 12b with corresponding reference numbers (nB: nano boron, cB: carbon-coated boron).

Material	Ref.	Material	Ref.	Material	Ref.
PbSe + TiB <sub>2</sub>	[90]	B <sub>4</sub> C + HfB <sub>2</sub>	[98]	Cu <sub>2</sub> Se + nB	[52]
TiB <sub>2</sub> + PVA	[90]	B <sub>4</sub> C + TiO <sub>x</sub>	[147]	Cu <sub>2</sub> Se + cB	[53]
SiB <sub>n</sub> + SiB <sub>6</sub>	[58]	B <sub>4</sub> C + Si + B	[186]	(Mg <sub>2</sub> Si) <sub>100</sub> B <sub>0.75</sub>	[183]
B <sub>4</sub> C + SiB <sub>n</sub>	[188]	ErB <sub>22</sub> C <sub>2</sub> N + ErB <sub>4</sub>	[35]	Bi <sub>0.5</sub> Sb <sub>1.5</sub> Te <sub>3</sub> + nB	[182]
B <sub>4</sub> C + TiB <sub>2</sub>	[187]	YB <sub>22</sub> C <sub>2</sub> N + VB <sub>2</sub>	[99]	Fe <sub>0.995</sub> B <sub>0.005</sub> Si <sub>2</sub>	[50]
B <sub>4</sub> C + 25 mol% TiB <sub>2</sub>	[47]	MgAg <sub>0.97</sub> Sb <sub>0.985</sub> B <sub>0.005</sub>	[184]		

## Acknowledgements

U.A. acknowledges the financial support provided by Koc University via Seed Funding.

## Conflict of Interest

The authors declare no conflict of interest.

## Keywords

borides, electronic transport, heat transport, refractory materials, thermo-electricity

Received: January 27, 2023

Revised: February 28, 2023

Published online:

- [1] V. Sharma, H. L. Kagdada, P. K. Jha, P. Śpiewak, K. J. Kurzydłowski, *Renewable Sustainable Energy Rev.* **2020**, *120*, 109622.
- [2] G. J. Snyder, E. S. Toberer, *Nat. Mater.* **2008**, *7*, 105.
- [3] I. Kim Sang, H. Lee Kyu, A. Mun Hyeon, S. Kim Hyun, W. Hwang Sung, W. Roh Jong, J. Yang Dae, H. Shin Weon, S. Li Xiang, H. Lee Young, G. J. Snyder, W. Kim Sung, *Science* **2015**, *348*, 109.
- [4] Y. Gelbstein, J. Davidow, S. N. Girard, D. Y. Chung, M. Kanatzidis, *Adv. Energy Mater.* **2013**, *3*, 815.
- [5] T. L. Aselage, D. Emin, In: *Chemistry, Physics, and Materials Science of Thermoelectric Materials. Fundamental Materials Research* (Eds: M. G. Kanatzidis, S. D. Mahanti, T. P. Hogan), Springer, Boston, MA **2003**.
- [6] J. T. Cahill, O. A. Graeve, *J. Mater. Res. Technol.* **2019**, *8*, 6321.
- [7] N. Orlovskaya, M. Lugovy, *Boron Rich Solids* (Ed: N. Orlovskaya, M. Lugovy), Springer, Dordrecht **2011**.
- [8] P. Jood, M. Ohta, A. Yamamoto, M. G. Kanatzidis, *Joule* **2018**, *2*, 1339.
- [9] Y. Tang, R. Hanus, S.-w. Chen, G. J. Snyder, *Nat. Commun.* **2015**, *6*, 7584.
- [10] E. Alleno, E. Zehani, O. Rouleau, *J. Alloys Compd.* **2013**, *572*, 43.
- [11] P. F. Qiu, J. Yang, R. H. Liu, X. Shi, X. Y. Huang, G. J. Snyder, W. Zhang, L. D. Chen, *J. Appl. Phys.* **2011**, *109*, 063713.
- [12] J. Yu, C. Fu, Y. Liu, K. Xia, U. Aydemir, T. C. Chasapis, G. J. Snyder, X. Zhao, T. Zhu, *Adv. Energy Mater.* **2018**, *8*, 1701313.
- [13] H. Zhu, R. He, J. Mao, Q. Zhu, C. Li, J. Sun, W. Ren, Y. Wang, Z. Liu, Z. Tang, A. Sotnikov, Z. Wang, D. Broido, D. J. Singh, G. Chen, K. Nielsch, Z. Ren, *Nat. Commun.* **2018**, *9*, 2497.
- [14] W. G. Zeier, S. Anand, L. Huang, R. He, H. Zhang, Z. Ren, C. Wolverton, G. J. Snyder, *Chem. Mater.* **2017**, *29*, 1210.
- [15] E. S. Toberer, C. A. Cox, S. R. Brown, T. Ikeda, A. F. May, S. M. Kauzlarich, G. J. Snyder, *Adv. Funct. Mater.* **2008**, *18*, 2795.
- [16] J. Zhang, L. Song, G. K. H. Madsen, K. F. F. Fischer, W. Zhang, X. Shi, B. B. Iversen, *Nat. Commun.* **2016**, *7*, 10892.
- [17] J. Wang, Y. He, N. E. Mordvinova, O. I. Lebedev, K. Kovnir, *Chem* **2018**, *4*, 1465.
- [18] H. Anno, T. Ueda, K. Okamoto, *J. Electron. Mater.* **2017**, *46*, 1730.
- [19] S. K. Deng, Y. Saiga, K. Suekuni, T. Takabatake, *J. Electron. Mater.* **2011**, *40*, 1124.
- [20] B. Sun, X. Jia, D. Huo, H. Sun, Y. Zhang, B. Liu, H. Liu, L. Kong, B. Liu, H. Ma, *J. Phys. Chem. C* **2016**, *120*, 10104.
- [21] M. Wagner, R. Cardoso-Gil, N. Oeschler, H. Rosner, Y. Grin, *J. Mater. Res.* **2011**, *26*, 1886.
- [22] M. Wagner-Reetz, R. Cardoso-Gil, Y. Grin, *J. Electron. Mater.* **2014**, *43*, 1857.
- [23] D. Kasinathan, M. Wagner, K. Koepf, R. Cardoso-Gil, Y. Grin, H. Rosner, *Phys. Rev. B* **2012**, *85*, 035207.
- [24] I. H. Warren, C. E. Price, *Adv. Energy Convers.* **1964**, *4*, 169.
- [25] S. Hirata, M. Ohtaki, K. Watanabe, *Ceram. Int.* **2020**, *46*, 25964.
- [26] D. Srivastava, C. Norman, F. Azough, D. Ekren, K. Chen, M. J. Reece, I. A. Kinloch, R. Freer, *J. Mater. Chem. A* **2019**, *7*, 24602.
- [27] S. Saini, H. S. Yaddanapudi, K. Tian, Y. Yin, D. Maggini, A. Tiwari, *Sci. Rep.* **2017**, *7*, 44621.
- [28] B. Jiang, X. Liu, Q. Wang, J. Cui, B. Jia, Y. Zhu, J. Feng, Y. Qiu, M. Gu, Z. Ge, J. He, *Energy Environ. Sci.* **2020**, *13*, 579.
- [29] Y. Li, G. Liu, T. Cao, L. Liu, J. Li, K. Chen, L. Li, Y. Han, M. Zhou, *Adv. Funct. Mater.* **2016**, *26*, 6025.
- [30] K. Zhao, P. Qiu, Q. Song, A. B. Blichfeld, E. Eikeland, D. Ren, B. Ge, B. B. Iversen, X. Shi, L. Chen, *Mater. Today Phys.* **2017**, *1*, 14.
- [31] G. K. Goyal, S. Mukherjee, R. C. Mallik, S. Vitta, I. Samajdar, T. Dasgupta, *ACS Appl. Energy Mater.* **2019**, *2*, 2129.
- [32] P. Gao, I. Berkun, R. D. Schmidt, M. F. Luzenski, X. Lu, P. Bordon Sarac, E. D. Case, T. P. Hogan, *J. Electron. Mater.* **2014**, *43*, 1790.
- [33] W. Liu, Q. Zhang, K. Yin, H. Chi, X. Zhou, X. Tang, C. Uher, *J. Solid State Chem.* **2013**, *203*, 333.
- [34] I. Gunjishima, T. Akashi, T. Goto, *Mater. Trans.* **2002**, *43*, 712.
- [35] T. Mori, T. Nishimura, *J. Solid State Chem.* **2006**, *179*, 2908.
- [36] M. Bouchacourt, F. Thevenot, *J. Mater. Sci.* **1985**, *20*, 1237.
- [37] A. Sussardi, T. Tanaka, A. U. Khan, L. Schlapbach, T. Mori, *J. Materials* **2015**, *1*, 196.
- [38] J. T. Cahill, M. Alberga, J. Bahena, C. Pisano, R. Borja-Urby, V. R. Vasquez, D. Edwards, S. T. Misture, O. A. Graeve, *Cryst. Growth Des.* **2017**, *17*, 3450.
- [39] H.-B. Ma, J. Zou, J.-T. Zhu, P. Lu, F.-F. Xu, G.-J. Zhang, *Acta Mater.* **2017**, *129*, 159.
- [40] M. Beauvy, *J. Less-Common Met.* **1983**, *90*, 169.
- [41] H. Suematsu, K. Kitajima, I. Ruiz, K. Kobayashi, M. Takeda, D. Shimbo, T. Suzuki, W. Jiang, K. Yatsui, *Thin Solid Films* **2002**, *407*, 132.
- [42] O. Sologub, Y. Matsushita, T. Mori, *Scr. Mater.* **2013**, *68*, 289.
- [43] A. A. Berezin, O. A. Golikova, M. M. Kazanin, T. Khomidov, D. N. Mirlin, A. V. Petrov, A. S. Umarov, V. K. Zaitsev, *J. Non-Cryst. Solids* **1974**, *16*, 237.
- [44] O. Sologub, L. Salamakha, B. Stöger, Y. Michiue, T. Mori, *Acta Mater.* **2017**, *122*, 378.
- [45] H. K. Kim, T. Nakayama, J. Shimizu, K. Kimura, *Mater. Trans.* **2008**, *49*, 0802120319.
- [46] H. Werheit, K. Flachbart, G. Pristáš, D. Lotnyk, V. Filipov, U. Kuhlmann, N. Shitsevalova, T. Lundström, *Semicond. Sci. Technol.* **2017**, *32*, 095015.
- [47] H. Werheit, *Solid State Sci.* **2011**, *13*, 1786.
- [48] H. Werheit, *Mater. Sci. Eng., B* **1995**, *29*, 228.
- [49] M. Adachi, K. Hirose, Y. Yamamoto, T. Takeuchi, *SEI Tech. Rev.* **2020**, *90*, 91.

- [50] Y. Isoda, Y. Shinohara, Y. Imai, I. A. Nishida, O. Ohashi, *Seventeenth International Conference on Thermoelectrics. Proceedings ICT98*, Nagoya, Japan **1998**, pp. 390–393.
- [51] R. Lackner, E. Bauer, P. Rogl, 2007 26th International Conference on Thermoelectrics, Jeju, Korea (South), **2007**, pp. 386–389.
- [52] S. M. K. Nazrul Islam, M. Li, U. Aydemir, X. Shi, L. Chen, G. J. Snyder, X. Wang, *J. Mater. Chem. A* **2018**, *6*, 18409.
- [53] M. Li, S. M. K. N. Islam, M. Yahyaoglu, D. Pan, X. Shi, L. Chen, U. Aydemir, X. Wang, *InfoMat* **2019**, *1*, 108.
- [54] K. Hayashi, W. Saito, K. Sugimoto, K. Ohoyama, K. Hayashi, N. Happo, M. Harada, K. Oikawa, Y. Inamura, Y. Miyazaki, *AIP Adv.* **2020**, *10*, 035115.
- [55] H. Chen, X. Zou, *Inorg. Chem. Front.* **2020**, *7*, 2248.
- [56] W. G. Fahrenholtz, J. Binner, J. Zou, *J. Mater. Res.* **2016**, *31*, 2757.
- [57] J. W. Simonson, S. J. Poon, *J. Alloys Compd.* **2010**, *504*, 265.
- [58] L. Chen, T. Goto, J. Li, T. Hirai, *Mater. Trans., JIM* **1996**, *37*, 1182.
- [59] D. Berthebaud, T. Nishimura, T. Mori, *J. Mater. Res.* **2010**, *25*, 665.
- [60] O. Lucía, P. Maussion, E. J. Dede, J. M. Burdío, *IEEE Trans. Ind. Electron.* **2014**, *61*, 2509.
- [61] G. Delaizir, G. Bernard-Granger, J. Monnier, R. Grodzki, O. Kim-Hak, P. D. Szkutnik, M. Soulier, S. Saunier, D. Goeuriot, O. Rouleau, J. Simon, C. Godart, C. Navone, *Mater. Res. Bull.* **2012**, *47*, 1954.
- [62] H. Kim, K. Kimura, *Mater. Trans.* **2011**, *52*, 41.
- [63] T. Fujima, H. Arimatsu, S. Miura, S. Yokoyama, K.-i. Takagi, *Solid State Sci.* **2015**, *47*, 51.
- [64] H. Sasaki, S. Miura, T. Fujima, K.-i. Takagi, *Solid State Sci.* **2012**, *14*, 1698.
- [65] S. Maruyama, Y. Miyazaki, K. Hayashi, T. Kajitani, T. Mori, *Appl. Phys. Lett.* **2012**, *101*, 152101.
- [66] M. Takeda, T. Fukuda, T. Miura, *Twenty-First International Conference on Thermoelectrics*, Long Beach, CA, USA **2002**, pp. 173–176.
- [67] J. K. Sonber, T. S. R. C. Murthy, C. Subramanian, S. Kumar, R. K. Fotedar, A. K. Suri, *Int. J. Refract. Met. Hard Mater.* **2011**, *29*, 21.
- [68] S. Angappan, M. Helan, A. Visuvasam, L. Berchmans, V. Ananth, *Ionics* **2011**, *17*, 527.
- [69] H. Werheit, 2006 25th International Conference on Thermoelectrics, Vienna, Austria **2006**, pp. 159–163.
- [70] T. Mori, *J. Phys.: Conf. Ser.* **2009**, *176*, 012036.
- [71] D. Berthebaud, A. Sato, Y. Michiue, T. Mori, A. Nomura, T. Shishido, K. Nakajima, *J. Solid State Chem.* **2011**, *184*, 1682.
- [72] G. A. Slack, D. W. Oliver, F. H. Horn, *Phys. Rev. B* **1971**, *4*, 1714.
- [73] S. Angappan, N. Kalaiselvi, R. Sudha, A. Visuvasam, *Int. Scholarly Res. Not.* **2014**, *2014*, 123194.
- [74] Y. Sato, T. Saito, K. Tsuchiya, M. Terauchi, H. Saito, M. Takeda, *J. Solid State Chem.* **2017**, *253*, 58.
- [75] I. Gunjishima, T. Akashi, T. Goto, *Mater. Trans.* **2001**, *42*, 1445.
- [76] M. A. Hossain, I. Tanaka, T. Tanaka, A. U. Khan, T. Mori, *J. Solid State Chem.* **2016**, *233*, 1.
- [77] T. Mori, T. Tanaka, *J. Solid State Chem.* **2006**, *179*, 2889.
- [78] K. Seevakan, S. Bharanidharan, *Int. J. Pure Appl. Math.* **2018**, *119*, 5743.
- [79] D. W. Oliver, G. D. Brower, *J. Cryst. Growth* **1971**, *11*, 185.
- [80] B. T. Lejeune, *Ph.D. Thesis*, Northeastern University, Boston, MA **2019**.
- [81] C. Bulfon, A. Leithe-Jasper, H. Sassik, P. Rogl, *J. Solid State Chem.* **1997**, *133*, 113.
- [82] W. P. R. George, C. H. L. Goodman, H. F. Sterling, R. W. Warren, *Phys. Status Solidi B* **1967**, *21*, 205.
- [83] V. N. Gurin, V. S. Sinelnikova, in *Boron and Refractory Borides* (Ed: V. I. Matkovich), Springer, Berlin, Heidelberg **1977**, pp. 377–389.
- [84] B. Bressel, B. Chevalier, J. Etourneau, P. Hagenmuller, *J. Cryst. Growth* **1979**, *47*, 429.
- [85] C. B. Finch, O. B. Cavin, P. F. Becher, *J. Cryst. Growth* **1984**, *67*, 556.
- [86] A. Jilani, M. Abdel-wahab, A. Hammad, *Advance Deposition Techniques for Thin Film and Coating* **2017**.
- [87] Y. Kumashiro, T. Yokoyama, K. Sato, Y. Ando, S. Nagatani, K. Kajiyama, *J. Solid State Chem.* **2000**, *154*, 33.
- [88] Y. Gong, Y. Zhang, M. Dudley, J. H. Edgar, P. Heard, M. Kuball, *J. Appl. Phys.* **2010**, *108*, 084906.
- [89] S. Sasaki, M. Takeda, K. Yokoyama, T. Miura, T. Suzuki, H. Suematsu, W. Jiang, K. Yatsui, *Sci. Technol. Adv. Mater.* **2005**, *6*, 181.
- [90] I. Malik, S. Banerjee, C. Gayner, A. Chowdhuri, K. K. Kar, *Ceram. Int.* **2018**, *44*, 10685.
- [91] D. C. Kim, J. S. Kim, B. H. Kim, Y. W. Park, C. U. Jung, S. I. Lee, *Phys. C* **2003**, *387*, 313.
- [92] K. F. Cai, E. Mueller, C. Drasar, A. Mrotzek, *Mater. Lett.* **2003**, *57*, 4251.
- [93] X. Yang, Z. Dai, Y. Zhao, S. Meng, *Comput. Mater. Sci.* **2018**, *147*, 132.
- [94] A. Bano, D. K. Pandey, A. Modi, N. K. Gaur, *Sci. Rep.* **2018**, *8*, 14444.
- [95] Y. Imai, M. Mukaida, M. Ueda, A. Watanabe, *Intermetallics* **2001**, *9*, 721.
- [96] M. Takeda, F. Domingo, T. Miura, T. Fukuda, *MRS Online Proc. Libr.* **2001**, *691*, 87.
- [97] B. Albert, K. Hofmann, In *Handbook of Solid State Chemistry* (Eds: R. Dronskowski, S. Kikkawa, A. Stein), **2017**.
- [98] J.-L. Innocent, D. Portehault, G. Gouget, S. Maruyama, I. Ohkubo, T. Mori, *Mater. Renewable Sustainable Energy* **2017**, *6*, 6.
- [99] A. Prytuliak, S. Maruyama, T. Mori, *Mater. Res. Bull.* **2013**, *48*, 1972.
- [100] W. N. Lipscomb, D. Britton, *J. Chem. Phys.* **1960**, *33*, 275.
- [101] J. Etourneau, J. P. Mercurio, P. Hagenmuller, in *Boron and Refractory Borides* (Ed: V. I. Matkovich), Springer, Berlin, Heidelberg **1977**.
- [102] A. B. Auskern, S. Aronson, *J. Chem. Phys.* **1968**, *49*, 172.
- [103] J. Etourneau, P. Hagenmuller, *Philos. Mag. B* **1985**, *52*, 589.
- [104] Z. P. Yin, W. E. Pickett, *Phys. Rev. B* **2008**, *77*, 035135.
- [105] A. Knappschneider, C. Litterscheid, D. Dzivenko, J. A. Kurzman, R. Seshadri, N. Wagner, J. Beck, R. Riedel, B. Albert, *Inorg. Chem.* **2013**, *52*, 540.
- [106] M. Yang, Y. Wang, J. Yao, Z. Li, J. Zhang, L. Wu, H. Li, J. Zhang, H. Gou, *J. Solid State Chem.* **2014**, *213*, 52.
- [107] S. Gabani, K. Flachbart, K. Siemensemeyer, T. Mori, *J. Alloys Compd.* **2020**, *821*, 153201.
- [108] E. Rausch, B. Balke, T. Deschauer, S. Ouardi, C. Felser, *APL Mater.* **2015**, *3*, 041516.
- [109] Y. Nishi, Y. Arita, K. Terao, T. Matsui, T. Nagasaki, *J. Nucl. Mater.* **2001**, *294*, 209.
- [110] O. M. Ozkendir, *Adv. J. Chem., Sect. B* **2020**, *2*, 48.
- [111] A. Knappschneider, C. Litterscheid, J. Brgoch, N. C. George, S. Henke, A. K. Cheetham, J. G. Hu, R. Seshadri, B. Albert, M. Tetraboride, *Chemistry* **2015**, *21*, 8177.
- [112] Y. Nishi, Y. Arita, T. Matsui, K. Iwasaki, T. Nagasaki, *J. Phys. Chem. Solids* **2005**, *66*, 652.
- [113] I. Veremchuk, T. Mori, Y. Prots, W. Schnelle, A. Leithe-Jasper, M. Kohout, Y. Grin, *J. Solid State Chem.* **2008**, *181*, 1983.
- [114] T. Mori, H. Borrmann, S. Okada, K. Kudou, A. Leithe-Jasper, U. Burkhardt, Y. Grin, *Phys. Rev. B* **2007**, *76*, 064404.
- [115] S. Lassoued, R. Gautier, J. F. Halet, in *Boron Rich Solids. NATO Science for Peace and Security Series B: Physics and Biophysics* (Eds: N. Orlovskaya, M. Lugovy), Springer, Dordrecht **2010**.
- [116] S. Lassoued, R. Gautier, A. Boutarfaia, J.-F. Halet, *J. Organomet. Chem.* **2010**, *695*, 987.
- [117] G. E. Grechnev, A. E. Baranovskiy, V. D. Fil, T. V. Ignatova, I. G. Kolobov, A. V. Logosha, N. Y. Shitsevalova, V. B. Filippov, O. Eriksson, *Low Temp. Phys.* **2008**, *34*, 921.
- [118] S. Flipo, H. Rosner, M. Bobnar, K. O. Kvashnina, A. Leithe-Jasper, R. Gumeniuk, *Phys. Rev. B* **2021**, *103*.

- [119] T. Akashi, T. Itoh, I. Gunjishima, H. Masumoto, T. Goto, *Mater. Trans.* **2002**, *43*, 1719.
- [120] S. Massidda, A. Continenza, T. M. de Pascale, R. Monnier, *Z. Phys. B: Condens. Matter* **1996**, *102*, 83.
- [121] M. Aono, S. Kawai, S. Kono, M. Okusawa, T. Sagawa, Y. Takehana, *J. Phys. Chem. Solids* **1976**, *37*, 215.
- [122] M. Takeda, T. Fukuda, F. Domingo, T. Miura, *J. Solid State Chem.* **2004**, *177*, 471.
- [123] R. W. Johnson, A. H. Daane, *J. Chem. Phys.* **1963**, *38*, 425.
- [124] H. Werheit, *Advances in Ceramic Armor X: A Collection of Papers Presented at the 38th International Conference on Advanced Ceramics and Composites January 27–31, 2014*, **2015**.
- [125] J. Stankiewicz, P. Rosa, P. Schlottmann, Z. Fisk, *Phys. Rev. B* **2016**, *94*.
- [126] M. Gürsoy, M. Takeda, B. Albert, *J. Solid State Chem.* **2015**, *221*, 191.
- [127] N. Takahashi, M. Terui, N. Ueda, M. Takeda, *ICT 2005. 24th International Conference on Thermoelectrics, 2005*, Clemson, SC, USA, 2005, pp. 423–425.
- [128] M. Takeda, M. Terui, N. Takahashi, N. Ueda, *J. Solid State Chem.* **2006**, *179*, 2823.
- [129] M. Takeda, T. Fukuda, Y. Kurita, *Thermoelectric Properties of Divalent Hexaborides*, **2003**.
- [130] T. Tynell, T. Aizawa, I. Ohkubo, K. Nakamura, T. Mori, *J. Cryst. Growth* **2016**, *449*, 10.
- [131] G. Guélou, M. Martirosyan, K. Ogata, I. Ohkubo, Y. Kakefuda, N. Kawamoto, Y. Kitagawa, J. Ueda, S. Tanabe, K. Maeda, K. Nakamura, T. Aizawa, T. Mori, *Materialia* **2018**, *1*, 244.
- [132] J. M. Lafferty, *J. Appl. Phys.* **1951**, *22*, 299.
- [133] K. Kaymura, M. Takeda, *IOP Conf. Ser.: Mater. Sci. Eng.* **2011**, *20*, 012007.
- [134] B. Lorenz, R. L. Meng, Y. Y. Xue, C. W. Chu, *Phys. Rev. B* **2001**, *64*, 052513.
- [135] J. Nagamatsu, N. Nakagawa, T. Muranaka, Y. Zenitani, J. Akimitsu, *Nature* **2001**, *410*, 63.
- [136] T. Mori, *JOM* **2016**, *68*, 2673.
- [137] H. Werheit, *J. Phys.: Conf. Ser.* **2009**, *176*, 012019.
- [138] Z. Xu, J. H. Edgar, D. C. Look, S. Baumann, R. J. Bleiler, S. H. Wang, S. E. Mohny, *J. Appl. Phys.* **2007**, *101*, 053710.
- [139] Y. Kumashiro, T. Yokoyama, A. Sato, Y. Ando, *J. Solid State Chem.* **1997**, *133*, 314.
- [140] K. Kumashiro, K. Hirata, K. Sato, T. Yokoyama, T. Aisu, T. Ikeda, M. Minaguchi, *J. Solid State Chem.* **2000**, *154*, 26.
- [141] T. Fujima, N. Shimizu, H. Arimatsu, *Materials* **2019**, *12*, 632.
- [142] S. Miura, H. Sasaki, K.-i. Takagi, T. Fujima, *J. Phys. Chem. Solids* **2014**, *75*, 951.
- [143] S. Maruyama, T. Nishimura, Y. Miyazaki, K. Hayashi, T. Kajitani, T. Mori, *Mater. Renewable Sustainable Energy* **2014**, *3*, 31.
- [144] L. Zhuang, Y. Lei, S. Chen, L. Hu, Q. Meng, *Appl. Surf. Sci.* **2015**, *328*, 125.
- [145] G. H. Kwei, B. Morosin, *J. Phys. Chem.* **1996**, *100*, 8031.
- [146] K. Rasim, R. Ramlau, A. Leithe-Jasper, T. Mori, U. Burkhardt, H. Borrmann, W. Schnelle, C. Carbogno, M. Scheffler, Y. Grin, *Angew. Chem., Int. Ed.* **2018**, *57*, 6130.
- [147] S. Roszeitis, B. Feng, H.-P. Martin, A. Michaelis, *J. Eur. Ceram. Soc.* **2014**, *34*, 327.
- [148] K. A. Schwetz, P. Karduck, *J. Less Common Metals* **1991**, *175*, 1.
- [149] P. Sauerstich, J. L. Watts, J. B. Vaney, P. C. Talbot, J. A. Alarco, I. D. R. Mackinnon, T. Mori, *Adv. Appl. Ceram.* **2020**, *119*, 97.
- [150] C. Wood, D. Emin, *Phys. Rev. B* **1984**, *29*, 4582.
- [151] T. L. Aselage, D. Emin, S. S. McCready, *Phys. Rev. B* **2001**, *64*, 054302.
- [152] V. Dornich, S. Reynaud, R. A. Haber, M. Chhowalla, *J. Am. Ceram. Soc.* **2011**, *94*, 3605.
- [153] K.-f. Cai, C.-W. Nan, X.-m. Min, *Mater. Sci. Eng., B* **1999**, *67*, 102.
- [154] T. L. Aselage, *High Temperature Thermoelectric Properties of Boron Carbide*, Materials Research Society, Warrendale, PA **1991**.
- [155] Y. W. Qin, S. K. Lu, *Adv. Mater. Res.* **2013**, *652–654*, 344.
- [156] K. Cai, C. W. Nan, Y. Paderno, D. S. McLachlan, *Solid State Commun.* **2000**, *115*, 523.
- [157] T. Akashi, I. Gunjishima, T. Goto, *Key Eng. Mater.* **2003**, *247*, 209.
- [158] M. Uehara, R. Shiraishi, A. Nogami, N. Enomoto, J. Hojo, *J. Eur. Ceram. Soc.* **2004**, *24*, 409.
- [159] J. L. Fan, Y. S. Wei, S. K. Lu, *Adv. Mater. Res.* **2013**, *690–693*, 602.
- [160] K.-f. Cai, C.-W. Nan, *Ceram. Int.* **2000**, *26*, 523.
- [161] F. Zhang, A. Leithe-Jasper, J. Xu, T. Mori, Y. Matsui, T. Tanaka, S. Okada, *J. Solid State Chem.* **2001**, *159*, 174.
- [162] F. Zhang, F. Xu, T. Mori, Q. Liu, A. Sato, T. Tanaka, *J. Alloys Compd.* **2001**, *329*, 168.
- [163] T. Mori, T. Nishimura, 2007 26th International Conference on Thermoelectrics, Jeju Island, **2007**, pp. 394–397.
- [164] T. Mori, T. Nishimura, K. Yamaura, E. Takayama-Muromachi, *J. Appl. Phys.* **2007**, *101*, 093714.
- [165] T. Mori, T. Nishimura, W. Schnelle, U. Burkhardt, Y. Grin, *Dalton Trans.* **2014**, *43*, 15048.
- [166] T. Mori, T. Shishido, K. Nakajima, *J. Electron. Mater.* **2009**, *38*, 1098.
- [167] K. Kudou, S. Fukuda, S. Okada, T. Mori, K. Iizumi, T. Shishido, Y. Mantani, *Jpn. J. Appl. Phys.* **2007**, *46*, 7803.
- [168] D. G. Cahill, H. E. Fischer, S. K. Watson, R. O. Pohl, G. A. Slack, *Phys. Rev. B* **1989**, *40*, 3254.
- [169] F. Zhang, T. Tanaka, *J. Cryst. Growth* **2004**, *271*, 159.
- [170] T. Mori, *J. Appl. Phys.* **2005**, *97*, 093703.
- [171] G. S. Nolas, G. A. Slack, D. T. Morelli, T. M. Tritt, A. C. Ehrlich, *J. Appl. Phys.* **1996**, *79*, 4002.
- [172] T. Zhong, H. Zhou, R. D. Horansky, C. Lee, V. B. Verma, A. E. Lita, A. Restelli, J. C. Bienfang, R. P. Mirin, T. Gerrits, *New J. Phys.* **2015**, *17*, 022002.
- [173] T. Mori, *J. Solid State Chem.* **2019**, *275*, 70.
- [174] P. Sauerstich, K. Tsuchiya, T. Tanaka, Y. Michiue, O. Sologub, S. Yin, A. Yoshikawa, T. Shishido, T. Mori, *J. Alloys Compd.* **2020**, *813*, 152182.
- [175] T. Mori, D. Berthebaud, T. Nishimura, A. Nomura, T. Shishido, K. Nakajima, *Dalton Trans.* **2010**, *39*, 1027.
- [176] A. Prytuliak, T. Mori, *J. Electron. Mater.* **2011**, *40*, 920.
- [177] T. Nakayama, J. Shimizu, K. Kimura, *J. Solid State Chem.* **2000**, *154*, 13.
- [178] G. A. Slack, K. Morgan, *Solid State Sci.* **2015**, *47*, 43.
- [179] T. Nakayama, H. Matsuda, K. Kimura, H. Ino, *IEEE J. Solid-State Circuits* **1997**, *133*, 342.
- [180] H. Werheit, U. Kuhlmann, T. Lundström, *J. Alloys Compd.* **1994**, *204*, 197.
- [181] Y. Takagiwa, N. Kuroda, E. Imai, I. Kanazawa, H. Hyodo, K. Soga, K. Kimura, *Mater. Trans.* **2016**, *57*, 1066.
- [182] G. Yang, R. Niu, L. Sang, X. Liao, D. R. G. Mitchell, N. Ye, J. Pei, J.-F. Li, X. Wang, *Adv. Energy Mater.* **2020**, *10*, 2000757.
- [183] M. Kubouchi, K. Hayashi, Y. Miyazaki, *Scr. Mater.* **2016**, *123*, 59.
- [184] W. Gao, X. Yi, B. Cui, Z. Wang, J. Huang, J. Sui, Z. Liu, *J. Mater. Chem. C* **2018**, *6*, 9821.
- [185] L. F. Wan, S. P. Beckman, *Phys. Chem. Chem. Phys.* **2014**, *16*, 25337.
- [186] B. Feng, H.-P. Martin, R. Hempel-Weber, A. Michaelis, *AIP Conference Proceedings*, **2012** pp. 315–318.
- [187] P. Ponnusamy, B. Feng, H.-P. Martin, P. Groen, *Mater. Today: Proc.* **2018**, *5*, 10306.
- [188] J. Li, T. Goto, T. Hirai, *Mater. Trans., JIM* **1999**, *40*, 314.



**Kivanc Saglik** obtained her B.Sc. and M.Sc. degrees from the Chemistry Department of Bogazici University and Koc University, Turkey, respectively. She is currently studying as a Ph.D. student at the Materials Science and Engineering Department of Nanyang Technological University and A\*STAR, Singapore.



**Busra Mete** is pursuing her Ph.D. in the Chemistry Department at the Max-Planck-Institute for Chemical Physics in Solids in Dresden, Germany. She earned her M.Sc. in Materials Science and Engineering from Koc University in Turkey and completed her undergraduate studies in Metallurgical and Materials Engineering at Yildiz Technical University.



**Ilayda Terzi** received her B.Sc. degree in Chemistry from the Izmir Institute of Technology. She earned her M.Sc. degree in Material Science and Engineering from Koç University in 2022. Currently, she is a Ph.D. student at the Institut Jean Lamour (IJL), Université de Lorraine in Nancy, France.



**Christophe Candolfi** is currently working at Institut Jean Lamour (IJL), Université de Lorraine at Nancy, France. After finishing his Ph.D. at Laboratoire de Physique des Matériaux, he joined the Chemistry Department of Max Planck Institute for Chemical Physics in Solids, Dresden, Germany, as a postdoctoral research associate for 3 years. He then joined IJL and was appointed as the director of the French Groupement d'Intérêt Scientifique on thermoelectricity in 2022.



**Umut Aydemir** is currently working at Koc University in Turkey. He earned his Ph.D. from the Chemistry Department of the Max Planck Institute for Chemical Physics in Solids in Dresden, Germany. After completing his Ph.D., he served as a postdoctoral research associate at both the California Institute of Technology and Northwestern University. In 2019, he joined Koc University and was appointed as the director of Koç University Boron and Advanced Materials Application and Research Center (KUBAM).